



**Strontium isotope shift in clay minerals,
epidote and geothermal fluid in the
Hellisheiði Geothermal Field, SW-Iceland**

Gísli Örn Bragason



**Faculty of Earth Sciences
University of Iceland
2012**

Strontium isotope shift in clay minerals, epidote and geothermal fluid in the Hellisheiði Geothermal Field, SW-Iceland

Gísli Örn Bragason

90 ECTS thesis submitted in partial fulfillment of a
Magister Scientiarum degree in Geology

Advisor(s)
Karl Grönvold
Sigurður Steinþórsson

Faculty Representative
Ingvi Gunnarsson

Faculty of Earth Science
School of Engineering and Natural Sciences
University of Iceland
Reykjavik, April 2012

Strontium isotope shift in clay minerals, epidote and geothermal fluid in the Hellisheiði Geothermal Field, SW-Iceland

90 ECTS thesis submitted in partial fulfillment of a *Magister Scientiarum* degree in Geology

Copyright © 2012 Gísli Örn Bragason
All rights reserved

Faculty of Earth Science
School of Engineering and Natural Sciences
University of Iceland
Askja, Sturlugötu 7
107 Reykjavík
Iceland

Telephone: 525 4000

Bibliographic information:

Gísli Örn Bragason, 2012,
Strontium isotope shift in clay minerals, epidote and geothermal fluid in the Hellisheiði Geothermal Field, SW-Iceland,
Master's thesis, Faculty of Earth Science, University of Iceland, pp. XX.

Reykjavík, Iceland, April 2012

Abstract

The large difference in the isotopic ratio $^{87}\text{Sr}/^{86}\text{Sr}$ between sea-water-derived meteoric water (0.70916) and that of the original reservoir rocks (0.70314) allows the detection of small amounts of Sr derived from meteoric water in alteration minerals formed. The broad picture confirmed here is that meteoric Sr is largely removed in the upper clay and zeolite zones but enough survives into the epidote-dominated zones. This causes a small but significant shift in the Sr-isotopic ratio in epidote downhole to the bottom of the geothermal wells. A few samples were found to have significantly higher $^{87}\text{Sr}/^{86}\text{Sr}$ than the surrounding samples and these samples coincide with the main aquifers feeding the geothermal wells. This suggests that the aquifer water flows fast enough through the system for equilibrium not to be attained with the bulk of the reservoir rocks.

Epidote is an abundant alteration mineral in high-temperature geothermal fields and one of the main index minerals used for the definition of temperature-dependent alteration zoning. In this study epidote from two drillholes, HE-50 and HE-51 in the Hellisheiði Geothermal Field was analyzed in detail by microprobe. As previously observed the epidote shows ubiquitous zoning of individual crystals with Fe-richer cores and Al-richer rims. Individual crystals at different depths span the entire compositional range observed throughout the geothermal wells.

The interpretation of this zoning is that the early Fe-rich epidote forms in the chlorite-epidote alteration zone in association with wairakite-prehnite-andradite. The growth of the Fe-poorer outer zone forms in the mineral assemblage hematite-prehnite-epidote. Epidote is a significant host for Sr within the deeper levels of the thermal fields while clay minerals and zeolites are the main hosts in the upper levels.

Eight samples of geothermal fluid from different sub-regions of the Hellisheiði geothermal fields were analyzed for $^{87}\text{Sr}/^{86}\text{Sr}$ and showed significant variation. Five samples showed ratios similar to the general deeper epidote values, two geothermal wells show ratios similar to those associated with the main aquifers, while one sample has ratio similar to those observed for the clays in the upper part of the system. Samples for wells HE-50 and HE-51 were not available but the results show clearly that studies of $^{87}\text{Sr}/^{86}\text{Sr}$ could be a worthwhile addition to the methods used for the interpretation of water circulation and water-rock interaction in geothermal fields.

Ágrip

Mikill munur er á samsætuhlutfallinu $^{87}\text{Sr}/^{86}\text{Sr}$ í grunnvatni, sem upprunnið er úr sjó (0,70916) og í gosbergi rekbeltanna (0,70314), sem gerir unnt að greina lítið magn af Sr úr grunnvatni í ummyndunarsteindum. Rannsóknin sýnir fram á að sjávar-Sr er að stórum hluta tekið upp í efri leir- og zeólítabelti en þó berst mælanlegt magn niður í epidótbeltið. Þetta veldur litlum en merkjanlegum breytingum á epidót niður eftir jarðlagasniðinu. Fáein sýni við vatnsæðar eru merkjanlega hærri í $^{87}\text{Sr}/^{86}\text{Sr}$ en nærliggjandi sýni. Þetta bendir til að vatnsæðar hafi nægilega hratt rennsli í gegnum kerfið til að viðhalda ójafnvægi við bergið.

Epidót er algeng ummyndunarsteind á háhitasvæðum og er ein þeirra einkennissteinda sem skilgreina hitaháð ummyndunarbelti. Í þessari rannsókn er epidót úr tveimur borholum, HE-50 og HE-51 á jarðhitasvæði Hellisheiðar, efnagreindur með örgreini þar sem kemur fram að hver einstakur kristall er með járnríkan kjarni en álríkan rima. Hver einstakur epidótkristall spannar allar breytingar sem eiga sér stað í epidót í öllu sniðinu á mismunandi dýpi. Járnríkur kjarni í epidót myndast í klórít-epidót ummyndunarbeltinu í jafnvægi við wairakít-prehnít-andratít. Járnsmátt ytra byrði epidót myndast í jafnvægi við hematít-prehnít. Strontíum er kristalsækið í epidót í neðri hluta jarðhitasvæða, en í efri hluta háhitasvæða safnast strontíum fyrir í leirsteindum, zeólítum og kalsíti.

Jarðhitavatni var safnað úr átta borholum og $^{87}\text{Sr}/^{86}\text{Sr}$ -hlutfall vatnsins greint. Fram kemur merkjanlegur munur: Fimm sýni sýndu hlutföll í jafnvægi við epidót í dýpri hluta kerfisins, tvær borholur sýndu hlutföll svipuð epidót úr vatnsæðum og ein hola sýndi hlutfall svipað og mældust í leirsteindum í efri hluta jarðhitakerfisins. Jarðhitavatnssýni úr HE-50 og 51 voru ekki aðgengileg en nærliggjandi holur sýndu svipuð hlutföll og epidót í vatnsæðum. Niðurstöður rannsóknarinnar benda til þess að $^{87}\text{Sr}/^{86}\text{Sr}$ í jarðhitavatni og ummyndunarsteindum geti gefið mikilvægar upplýsingar um hringrás vatns og samspil vatns og bergs á jarðhitasvæðum.

Table of Contents

List of Figures	vi
List of Tables.....	viii
Abbreviations.....	ix
Acknowledgements	xi
1 Introduction.....	1
1.1 Geology and geothermal alteration patterns	2
2 Sampling and analytical techniques.....	9
3 Analytical Results	13
3.1 Whole rock analysis.....	13
3.2 Microprobe analysis.....	15
3.3 Strontium isotopes analyses	18
4 Discussion	21
4.1 Formation and paragenesis of epidote	21
4.2 Strontium isotopes	27
4.2.1 $^{87}\text{Sr}/^{86}\text{Sr}$ in the drill cuttings.....	27
4.2.2 Geothermal fluid	28
5 Summary and conclusions.....	31
References.....	35
Appendix I.....	39
Apendix II.....	45

List of Figures

Fig. 1 Geology map of Hellisheiði Geothermal Field based on geology map from Sæmundsson (1995). On the map is marked the location and direction of the drillholes.	3
Fig. 2 Alteration zones in HE-50 and HE-51. Depth is measured in meters above and below sea level (Gunnarsdóttir et al, 2010a; 2010b; Mattíasdóttir and Ingólfsson, 2010a;2010b).....	4
Figure 3 Lithology of wells HE-50 and HE-51.(Gunnarsdóttir et al, 2010a; 2010b; Mattíasdóttir and Ingólfsson, 2010a;2010b).	6
Fig. 4 Chemical composition of whole rock (cuttings) from wells HE-50 (triangle) and HE-51 (squares) in Hellisheiði Geothermal Field. Filled objects are isotope samples.....	14
Fig. 5 Section A-B shows the traverse of the probe scan. The epidote column shows Fe(III) rich cores and Al-rich rims. Epidote from vein filling at -1076 m b.s.l.	16
Fig. 6 Section shows the traverse of the probe scan. The epidote column show Ti rich cores and Sr-rich rims. Epidote from vein filling at -1076 m b.s.l.....	17
Fig. 7 Epidote Ps ($n_{Fe} / (n_{Al} / n_{Fe})$) plotted against depth from wells HE-50 and HE-51 in Hellisheiði geothermal system. Gray lines indicate RN-17 from Reykjanes Geothermal Field (Freedman et al., 2009) (Explanation for Ps is given on page 19).....	17
Fig. 8 SEM microphotograph, backscatter image, baseline length 350 μ m. Some of the typical features of hydrothermal epidote paragenesis are displayed in the figure. The light core of the epidote needles represent iron rich composition while the darker margins are iron poor. Prehnite is in a close relation to the epidote and both phases are embedded in a matrix of clay minerals where the ever-present hydrothermal feldspars are also present. Note the dendritic titanomagnetite cluster in the lower left and the titanomagnetite inclusion in the epidote. Sample from HE-50 at -1713 m b.s.l.	22
Fig. 9 Epidote-Prehnite vein with andradite garnet, HE-50 at -827 m b.s.l.	22
Fig. 10 SEM microphotograph, backscatter image. Wairakite (upper left) is replaced by prehnite with well evolved crystal phases. Epidote grows into the prehnite mass along a reaction zone, HE-51 at -1670 m b.s.l.	23
Fig. 11 Primary plagioclase replaced by epidote in HE-51 at -1885 m b.s.l. SEM microphotograph, backscatter image, baseline length 550 μ m. Virtually	

unzoned epidote (upper right) replacing plagioclase. The reaction rim has to be fed with Fe(III) from the fluid.	24
Fig. 12 Epidote associated with actinolite, albite, K-feldspar and titanite from -1559 m b.s.l from HE-50. SEM microphotograph, backscatter image. Typical paragenesis of epidote in the epidote actinolite facies. Actinolite grows along veins while the matrix is rich in albite with occasional K-fel. The hydrothermal alkali feldspars are all that remain of the igneous plagioclase that was replaced by epidote.....	25
Fig. 13 Strontium isotope ratios plotted against depth in well HE-50 and HE-51. Dotted line are feed points.....	28
Fig. 14 Strontium isotope ratios in geothermal water plotted against distance in meters.....	30

List of Tables

Table 1 List of samples in well HE-50.....	10
Table 2 List of samples in well HE-51.....	11
Table 3 Representative epidote analyses from Hellisheiði Geothermal Field	15
Table 4 Strontium isotope ratios in clay fraction from HE-50 and HE-51	18
Table 5 Strontium isotope ratios in epidote from HE-50 and HE-51.....	19
Table 6 Strontium isotope ratios in geothermal water from Hellisheiði Geothermal Field.....	19
Table 7 Major and trace elements in HE-50 and HE- 51	39
Table 8 Represent prehnite analyses from Hellisheiði Geothermal Field.....	45

Abbreviations

Epidote = Ep

Prehnite = Prh

Chlorite = Chl

Albite = Ab

Kalium feldspar = K-fel

Plagioclase = Pl

Wairakite = Wai

Actionolite = Act

Garnet = Grt

Last Glacial Maxium = LGM

Acknowledgements

I thank the Iceland Geosurvey and GEORG for funding most of this project. Also, I wish to thank my supervisors and the staff at Iceland Geosurvey and Orkuveitan for help and suggestions during this project. Guðrún Sverrisdóttir and Gylfi Sigurðsson at the Institute of Earth Sciences are thanked for great help in isotope analysis. Ingvi Gunnarsson for help with collected water sample from wells. Last but not least, I thank my beloved ones for help and patience during this work.

1 Indroduction

High temperature geothermal systems at diverging plate boundaries arise from thermal anomalies within rift-zone crust. Geothermal fields in Iceland are fed by meteoric water – the exceptions from this are the low elevation geothermal fields on the Reykjanes peninsula that are wholly or partly fed directly by seawater.

The average chemical composition of rain in Iceland is close to 1‰ seawater. Seawater contains 13 mg/l of Sr and rainwater with 1‰ seawater thus contains 0.013 mg/l of strontium. Although a low concentration, as compared with the about 130 mg/kg of Sr contained in average olivine tholeiite of the Western Rift-Zone (WRZ) in Iceland, the assimilation of Sr from rain into rock can be detected by precision isotope $^{87}\text{Sr}/^{86}\text{Sr}$ ratio measurements.

Icelandic rocks generally have $^{87}\text{Sr}/^{86}\text{Sr}$ isotope ratios distinctively higher relative to the submerged oceanic ridges towards south and north. It is well documented that the common $^{87}\text{Sr}/^{86}\text{Sr}$ ratio of basalts in the (WRZ) is around 0.70314 and, therefore, an addition of Sr from seawater/meteoric water with $^{87}\text{Sr}/^{86}\text{Sr}$ ratio of 0.70916 (Elderfield & Greaves, 1981) can be detected in trace amounts. This is the basis for the use of Sr as a tracer for rain water/rock interaction. In round numbers the average precipitation in Iceland is 1000 mm/yr which implies that 1 m³ of olivine tholeiite that collects all Sr from rain during 2700 yrs has doubled its Sr content to 260 mg/kg and its $^{87}\text{Sr}/^{86}\text{Sr}$ ratio would be close to 0.7062.

A geothermal system in a rift zone is active within a pile of subsiding basaltic lavas and hyaloclastites that have suffered alteration ranging from surface weathering through progressive alteration to an almost pervasive hydrothermal alteration in the epidote – actinolite zone. Also, the lava pile is cut by dykes and intrusions that assume the alteration stage prevalent within each zone. The water involved is geothermal fluid already equilibrated with earlier surroundings. As shown in this and earlier studies this uptake of Sr from rainwater into minerals primarily occurs within the uppermost crustal layer within the initial zeolite alteration zone. It is therefore important to look for Sr isotope shift towards seawater in alteration minerals with high affinity for strontium. Common smectite clay minerals such as montmorillonite and vermiculite are examples of minerals that are used for Sr-cleanup of radioactive waste and it is obvious that the clay fraction of the upper alteration zones is ideal for tracing the path of meteoric Sr. Epidote that later appears in the chlorite epidote zone has high affinity for Sr, crystals with SrO on the percent scale are common. The high affinity of epidote for Sr makes it ideal for tracing the meteoric water/rock interaction.

The present work uses drill cutting samples from geothermal wells HE-50 and HE-51 from one of the subsystems of the Hellisheiði Geothermal Field. The composition of epidote and its paragenesis is defined in considerable detail and show an interesting systematic variation that is dependent on variable mineral assemblages during the progressive alteration stages. The path of Sr through the geothermal system can be traced through the Sr isotopic composition of clay fraction and epidote is reported and the relations between isotopic composition and burial depth and hence alteration stage is outlined.

The final result of the meteoric water flow through the geothermal system and its heat extraction and reactions with the reservoir rocks is the outflow from the drillholes.

Geothermal water samples were collected and Sr isotopic ratios analyzed from a number of Hellisheiði subsystems. These results should reflect the overall interaction of the meteoric water within the system and thus possibly reflect the rate of water flow through the system. The results show a systematic decrease from north to south presumably reflecting the rate of flow through the various subsystems of the Hellisheiði Geothermal Field.

1.1 Geology and geothermal alteration patterns

The Hellisheiði geothermal field sits in the southern flanks of Hengill volcanic center (803 m a.s.l.) that fills the about 4 km wide WRZ-graben with hyaloclastites and lavas rising to about 500 m above the rift-zone surroundings. The time constraint indicates the Saalian, Eemian and Weichselian, when Hengill evolved into a volcanic center beginning three to four hundred thousand years ago. (Sæmundsson,1995; Franzson et al., 2010)

Rocks of the WRZ including the Hengill volcanic center are mostly olivine tholeiite. (Hansteen, 1999; Larsson et al., 2002; Trönnnes,1990). Few outcrops of evolved rocks, ranging towards rhyodacite composition are known within the Hengill volcano and evolved rocks appear in well-cuttings from the area. (Nielsson, 2011)

The Hengill geothermal area is generally applied to the whole geothermal activity of the Hengill volcano. This divides into a number subsystems and the present study focuses mainly on part of the Hellisheiði field and especially on two boreholes HE-50 and HE-51 in the eastern part of the presently exploited Hellisheiði field.

The principal heat source of the Hengill geothermal activity is assigned to abundant dyke injections beneath the Hengill volcano including the Hellisheiði Geothermal Field. Fig. 1, shows the main geological features of the Hellisheiði Geothermal Field and location of geothermal wells used in this project and with their direction. Drill cuttings come from wells HE-50 and HE-51 but geothermal fluid samples for Sr isotope analyses include other subareas of the Hellisheiði Geothermal Field.

Stratigraphy of the Hengill area is made up of interlaced series of basaltic hyaloclastites, breccia and basaltic lavas (Helgadóttir, 2010). These stratigraphic sequences illustrate the interplay between eruptive conditions during the glacial and interglacial conditions during the Quaternary. The effusive units are likely to reflect rifting events of the volcanic fissure swarms during the build up of the volcano. Subglacially formed hyaloclastite ridges are the main topographical feature of the Hengill rift segment. During interglacials, including the Holocene, lava flows from fissure eruptions, fill in ancient and recent valleys between the ridges resulting in a rift surface with marked age difference among closely spaced eruption units. Stratigraphic units revealed by cuttings from geothermal drilling in the area include hyaloclastites down to 800-1000 m b.s.l. while lavas and dykes increase with depth and dominate the deeper levels.

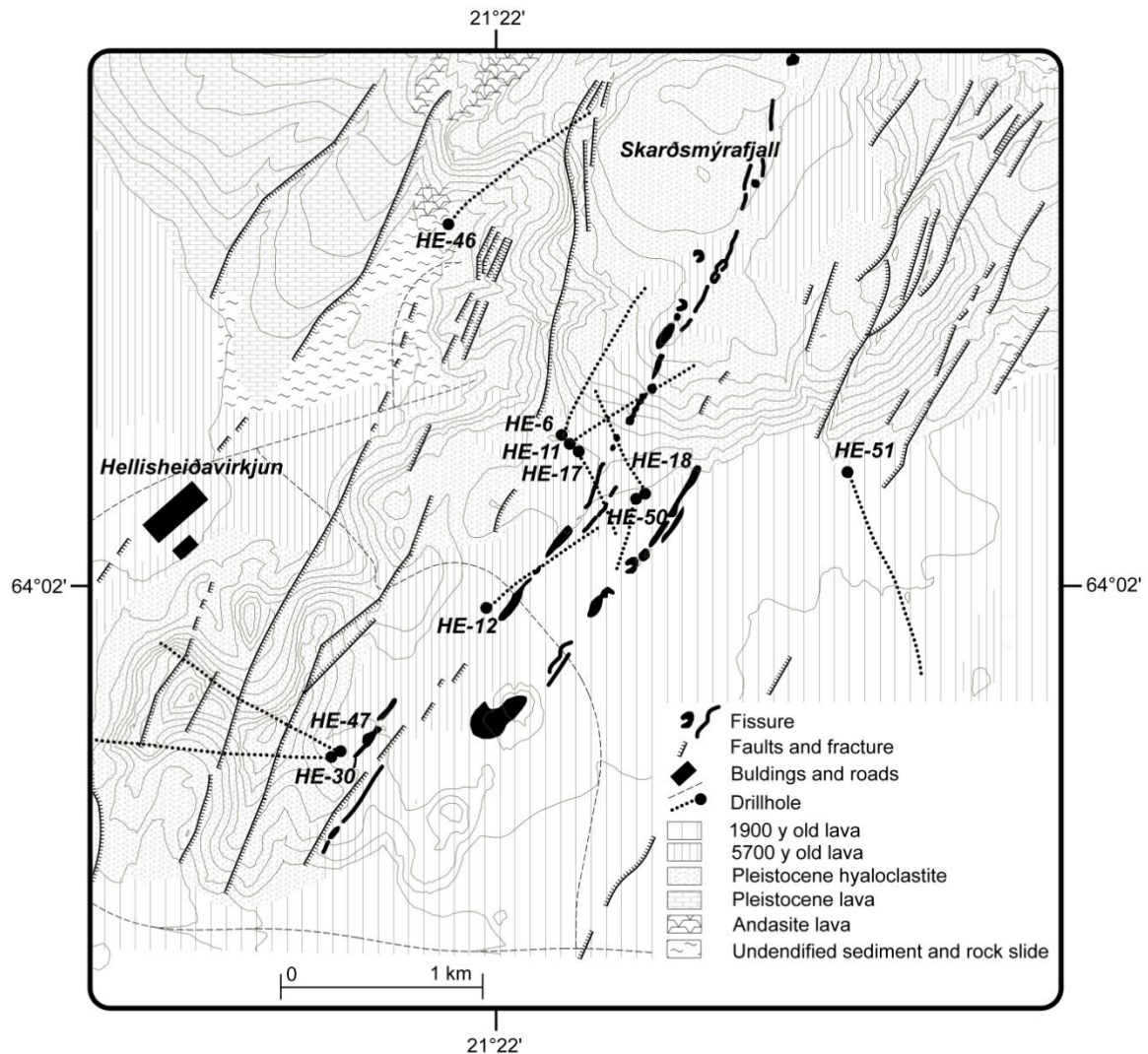


Fig. 1 Geology map of Hellisheiði Geothermal Field based on geology map from Sæmundsson (1995). On the map is marked the location and direction of the drillholes.

Repeated ice load and unloading during deglaciations seriously affect the thermal gradients within the geothermal fields increasing the gradients during loading and lowering during deglaciations. The geothermal alteration of the Hellisheiði Geothermal Field is thus assumed to have reached maximum during the last glaciation followed by cooling during the Holocene. The observed high-temperature alteration at shallow depth is possibly caused by elevated hydrostatic pressure by ice-load during the Pleistocene (Fridleifsson & Elders, 2005). This pattern is then complicated around the Holocene volcanic fissures (5000 and 2000 year old) where localized heating is assumed to favour renewed geothermal activity. (Franzson et al., 2005). Geothermal wells HE-50 and HE-51 (fig. 2 and fig. 3) cut original stratigraphic sequences of hyaloclastites in the upper part and lavas and intrusions in the lower half in a similar way as the generalized scenario described above (Gunnarsdóttir et al, 2010a; 2010b; Mattíasdóttir and Ingólfsson, 2010a; 2010b).

Regular alteration zoning (fig. 2) has formed in the geothermal areas in Iceland by reaction of geothermal fluids with the host rock and depends on increasing temperature with depth. This alteration zoning is defined by one or more index minerals i.e. smectite, zeolite,

chlorite, epidote and actinolite and distinct mineral assemblages (Tomasson & Kristmannsdottir, 1972; 1979; Franzson, 1998). Fig. 3 shows the variable depth and thickness of the alteration zones in drillholes HE-50 and HE-51 possibly reflecting the different locations of the drillholes may be assumed to derive from the fluctuation of isotherms during glacial- and interglacial periods.

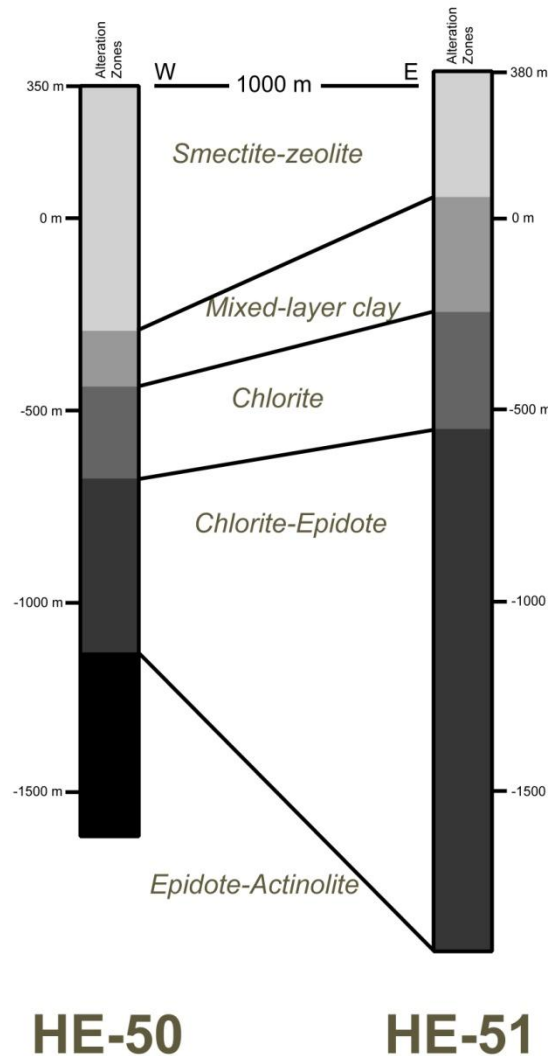


Fig. 2 Alteration zones in HE-50 and HE-51. Depth is measured in meters above and below sea level (Gunnarsdóttir et al, 2010a; 2010b; Mattíasdóttir and Ingólfsson, 2010a;2010b)

Smectite-zeolite alteration zone is formed from the surface to a depth about 300 - 500 m. The mineral assemblage is dominated by the variety of zeolites and the clay mineral smectite which is stable up to 200°C. Wairakite and quartz are first observed in this zone and calcite is usually abundant.

At the temperature of about 200°C smectite becomes unstable and its inclusion of chlorite layers leads to the formation of the mixed layer alteration zone. Although this alteration zone may be locally narrow it is well documented by XRD analysis. The mixed-layer minerals are gradually transformed into chlorite and wairakite with rising temperature to about 220°C

High grade mineral alteration assemblages start with the formation of chlorite in a zone where prehnite also becomes a dominant phase. Wairakite, calcite and quartz are found throughout this zone which also marks the appearance of epidote and andradite at temperatures above 250°C.

The fourth zone is characterized with epidote as index mineral and prehnite, quartz, calcite, albite, wollastonite and chlorite occur as well. Andradite garnet is found in this zone, frequently as inclusions in prehnite and epidote.

The appearance of actinolite marks the onset of the epidote-actinolite zone. Temperature has generally reached about 300°C and epidote occurs throughout this zone. The mineral assemblages include quartz, wollastonite, prehnite and albite. Calcite is usually absent and dissolution of igneous plagioclase and clinopyroxene is very noticeable.

The geothermal wells studied here are similar in broad terms. Well HE-50 shows progressive alteration zoning from smectite-zeolite to epidote-actinolite while easternmore HE-51 shows slower progressive alteration at depth with a significantly thicker epidote-chlorite zone

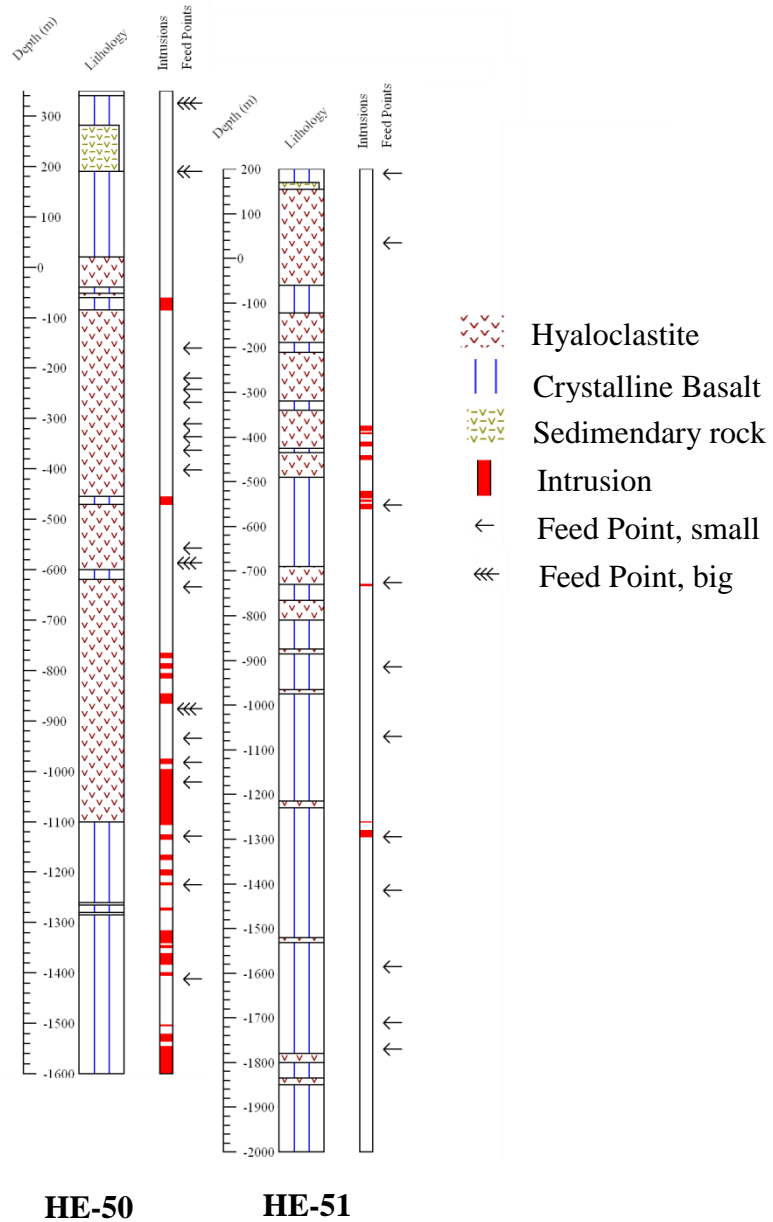


Figure 3 Lithology of wells HE-50 and HE-51. (Gunnarsdóttir et al, 2010a; 2010b; Mattíasdóttir and Ingólfsson, 2010a; 2010b).

2 Sampling and analytical techniques

A list of samples that were analyzed from drillholes HE-50 and HE-51 is shown in Table 1 where the stratigraphic depth, assumed lithofacies and classification into alteration zones is also noted. These can be used to display the main lines in whole rock composition but can not be taken to represent detailed silicate chemistry of single stratigraphic units. However, these samples are adequate for defining igneous mineral assemblages of the rock as well as representing the alteration minerals and their relation to the host rock.

Each sample was washed in Grade I water (<18 ohm) and then split for whole-rock chemical analysis and for mineral separation. Epidote crystals were identified under stereomicroscope and hand-picked for microprobe and isotopic analysis. A few epidote crystals from each sample were selected for microprobe analysis while the remaining epidote fraction was powdered for dissolution and Sr separation for isotopic analysis.

The clay fraction of the cuttings was separated by forming a clay suspension in water by ultrasonic agitation and subsequent withdrawal of the clay. The purity of the clay fraction may be slightly affected by inclusion of small amounts of calcite.

Well cuttings that may represent a stratigraphic thickness of about 2 m can be used to display the main outline in whole rock composition but cannot be taken to represent detailed whole rock silicate chemistry of single stratigraphic units. However, these samples are adequate for defining igneous mineral assemblages of the rock as well as alteration minerals and their relation to the host rock.

Whole rock chemical analyses were made on powdered samples fluxed in two parts lithium-metaborate at 1000°C for 30 min. The resulting glass bead was dissolved in a complexing acid mixture consisting of 5 Vol% HNO₃, 1.33 Vol% HCl and 1.33 Vol% saturated oxalic acid. Analytical solutions were adjusted to 1% dissolved solids corresponding to sample dilution of 1/300. Major and several trace elements were analyzed on a ICP-OES simultaneous spectrometer (SPECTRO CIROS).

Electron microprobe and SEM analyses were made on carbon-coated polished minerals and cuttings molded in epoxy. Running conditions were 15KV at 15 nA beam current using a collection of microprobe standards. Sr was measured using the L α peak with counting time for the wavelength dispersive peak and background times of 60 s. Standards for electron microprobe analysis of Sr were made by the preparation of a series of Sr-enriched dacitic glass containing up to 6 Wt% SrO. The mineral analyses were done on the SEMQ microprobe at Institute of Earth Sciences but the backscattered images were done at the SEM facilities at Innovation Center Iceland.

Strontium for isotopic analysis was separated after sample dissolution in HF and HNO₃. The solution was then saturated with HF and the precipitated fluorides were collected by centrifugation. After washing and repeated separation the solid fluorides were dissolved in 12M HNO₃ and run through Empore® Sr-Rad-Disk® (® 3M Company). After washing with 12M HNO₃ the moist disk was neutralized with ammonia and the adsorbed Sr was then eluted with dilute basic EDTA solution.

After evaporation to dryness the Sr sample was taken up in 1% HNO₃ for isotopic analysis.

Extraction of Sr from separated clay fractions was made by leaching the clay in 2M HNO₃ before extraction of Sr on Sr-Rad-Disk® was made.

Sr isotopic analysis of water was made after pre-concentration of Sr from acidified water on a small Dowex 50X8 column. Sr was eluted with 12M HNO₃ and then separated on a Sr-Rad-Disk® by the method outlined above.

Table 1 List of samples in well HE-50

Sample	Depth (m b.s.l)	Lithology	Alteration zones
HE-50 152	152	Glassy basalt	Smectite-zeolite
HE-50 0	0	Basaltic tuff	Smectite-zeolite
HE-50-50	-50	Fine crystalline basalt	Smectite-zeolite
HE-50-100	-100	Basaltic breccia	Smectite-zeolite
HE-50-145	-145	Basaltic breccia	Smectite-zeolite
HE-50-195	-195	Basaltic breccia	Smectite-zeolite
HE-50-245	-245	Basaltic breccia	Smectite-zeolite
HE-50-295	-295	Basaltic breccia	Mixlayer clay
HE-50-344	-344	Basaltic tuff	Mixlayer clay
HE-50-392	-392	Basaltic tuff	Mixlayer clay
HE-50-441	-441	Basaltic tuff	Chlorite
HE-50-489	-489	Basaltic tuff	Chlorite
HE-50-537	-537	Basaltic tuff	Chlorite
HE-50-586	-586	Basaltic tuff	Chlorite
HE-50-634	-634	Basaltic breccia	Chlorite-Epidote
HE-50-682	-682	Basaltic breccia	Chlorite-Epidote
HE-50-731	-731	Basaltic breccia	Chlorite-Epidote
HE-50-779	-779	Basaltic tuff	Chlorite-Epidote
HE-50-827	-827	Basaltic tuff	Chlorite-Epidote
HE-50-876	-876	Basaltic breccia	Chlorite-Epidote
HE-50-924	-924	Medium crystalline basalt	Chlorite-Epidote
HE-50-972	-972	Basaltic breccia	Chlorite-Epidote
HE-50-1021	-1021	Basaltic breccia	Chlorite-Epidote
HE-50-1070	-1070	Medium crystalline basalt	Chlorite-Epidote
HE-50-1118	-1118	Medium crystalline basalt	Chlorite-Epidote
HE-50-1167	-1167	Medium crystalline basalt	Epidote-Actionolite
HE-50-1216	-1216	Fine crystalline basalt	Epidote-Actionolite
HE-50-1265	-1265	Basaltic breccia	Epidote-Actionolite
HE-50-1313	-1313	Glassy basalt	Epidote-Actionolite
HE-50-1363	-1363	Glassy basalt	Epidote-Actionolite
HE-50-1450	-1412	Glassy basalt	Epidote-Actionolite
HE-50-1460	-1460	Glassy basalt	Epidote-Actionolite
HE-50-1509	-1509	Medium crystalline basalt	Epidote-Actionolite
HE-50-1559	-1559	Medium crystalline basalt	Epidote-Actionolite
HE-50-1607	-1607	Medium crystalline basalt	Epidote-Actionolite

Table 2 List of samples in well HE-51

Sample	Depth (m b.s.l)	Lithology	Alteration zones
HE-51 121	121	Basaltic tuff	Smectite-zeolite
HE-51 85	85	Basaltic tuff	Smectite-zeolite
HE-51 35	35	Basaltic breccia	Mixlayer clay
HE-51-15	-15	Basaltic tuff	Mixlayer clay
HE-51-75	-75	Basaltic breccia	Mixlayer clay
HE-51-122	-112	Glassy basalt	Mixlayer clay
HE-51-161	-161	Basaltic breccia	Mixlayer clay
HE-51-208	-208	Fine-medium crystalline basalt	Mixlayer clay
HE-51-251	-251	Basaltic breccia	Mixlayer clay
HE-51-295	-295	Basaltic tuff	Chlorite
HE-51-338	-338	Crystalline basalt	Chlorite
HE-51-382	-382	Crystalline basalt	Chlorite
HE-51-425	-425	Basaltic breccia	Chlorite
HE-51-468	-468	Basaltic tuff	Chlorite
HE-51-510	-510	Glassy basalt	Chlorite
HE-51-552	-552	Fine crystalline basalt	Chlorite
HE-51-595	-595	Glassy basalt	Chlorite-Epidote
HE-51-638	-638	Glassy basalt	Chlorite-Epidote
HE-51-681	-681	Basaltic tuff	Chlorite-Epidote
HE-51-724	-724	Basaltic breccia	Chlorite-Epidote
HE-51-767	-767	Basaltic breccia	Chlorite-Epidote
HE-51-810	-810	Medium crystalline basalt	Chlorite-Epidote
HE-51-853	-853	Medium crystalline basalt	Chlorite-Epidote
HE-51-896	-896	Fine crystalline basalt	Chlorite-Epidote
HE-51-939	-939	Basaltic breccia	Chlorite-Epidote
HE-51-982	-982	Fine-medium crystalline basalt	Chlorite-Epidote
HE-51-1025	-1025	Fine-medium crystalline basalt	Chlorite-Epidote
HE-51-1068	-1068	Fine-medium crystalline basalt	Chlorite-Epidote
HE-51-1111	-1111	Fine-medium crystalline basalt	Chlorite-Epidote
HE-51-1154	-1154	Fine-medium crystalline basalt	Chlorite-Epidote
HE-51-1197	-1197	Fine-medium crystalline basalt	Chlorite-Epidote
HE-51-1240	-1240	Fine-medium crystalline basalt	Chlorite-Epidote
HE-51-1283	-1283	Medium crystalline basalt	Chlorite-Epidote
HE-51-1326	-1326	Fine-medium crystalline basalt	Chlorite-Epidote
HE-51-1369	-1369	Fine-medium crystalline basalt	Chlorite-Epidote
HE-51-1412	-1412	Fine-medium crystalline basalt	Chlorite-Epidote
HE-51-1455	-1455	Fine-medium crystalline basalt	Chlorite-Epidote
HE-51-1498	-1498	Fine-medium crystalline basalt	Chlorite-Epidote
HE-51-1541	-1541	Medium crystalline basalt	Chlorite-Epidote
HE-51-1584	-1584	Fine crystalline basalt	Chlorite-Epidote
HE-51-1627	-1627	Fine crystalline basalt	Chlorite-Epidote
HE-51-1670	-1670	Fine-medium crystalline basalt	Chlorite-Epidote
HE-51-1713	-1713	Fine-medium crystalline basalt	Chlorite-Epidote
HE-51-1756	-1756	Medium crystalline basalt	Chlorite-Epidote
HE-51-1799	-1799	Basaltic tuff	Chlorite-Epidote
HE-51-1842	-1842	Basaltic breccia	Chlorite-Epidote
HE-51-1885	-1885	Fine-medium crystalline basalt	Chlorite-Epidote
HE-51-1928	-1928	Fine crystalline basalt	Chlorite-Epidote

3 Analytical Results

3.1 Whole rock analysis

Whole rock analysis of cuttings from Well HE-50 and Well HE-51 are listed in Table 1 and shown in Fig. 4 for a few major elements and Sr content as a function of depth with the whole rock values for both wells broadly similar.

Below 500 m b.s.l. depth the whole rock composition is all basaltic with a fairly restricted compositional range. Below 1000 m b.s.l. rock type is dominated by crystalline basalts – lava flows and intrusions. Between 1000 and 500 m b.s.l. the rock type is alternating layers of hyaloclastites and crystalline basalts. In the uppermost 500 m b.s.l. the dominating rock type is hyaloclastites that are significantly more altered than the crystalline basalts. These samples show a significantly greater variability in composition with SiO₂ ranging up to 57.7 % and MgO down to 3.7%. Some of the compositional scatter may be influenced by the intense alteration but comparison with fresh intermediate rocks from the Hengill area suggests that the variation observed mainly reflects genuine variation in the host rocks.

One of the characteristics of Icelandic Central Volcanoes is the presence of evolved rocks forming an igneous suite ranging from olivine tholeiites and up to rhyolites. This contrasts with the surrounding lava shields dominated by more primitive olivine tholeiites as exemplified by interglacial lava shields to the west and east of Hengill and Holocene lava shields to the north and south. The results from the cuttings from HE-50 and HE-51 agree well with previous suggestion that the Hengill Central Volcano started forming with more evolved rock types 0.3-0.4 million years ago and represented in the upper 500 m b.s.l. of the drillholes (Nielsson, 2011).

This change in volcanic activity is also reflected in the Sr content (fig, 4) with higher and much more variable SrO content in the upper 500 m b.s.l. complicating interpretation of the Sr budget of the geothermal system by introducing more rocks with higher Sr into the system. It should also be noted that some of the olivine tholeiites from the surrounding areas have significantly lower ⁸⁷Sr/⁸⁶Sr (down to 0.70301 (Karl Gronvold per. com.)) than the most common average of 0.70314 of the Icelandic rift zone tholeiites – this may be relevant for the general interpretation of Sr isotope shift due to alteration.

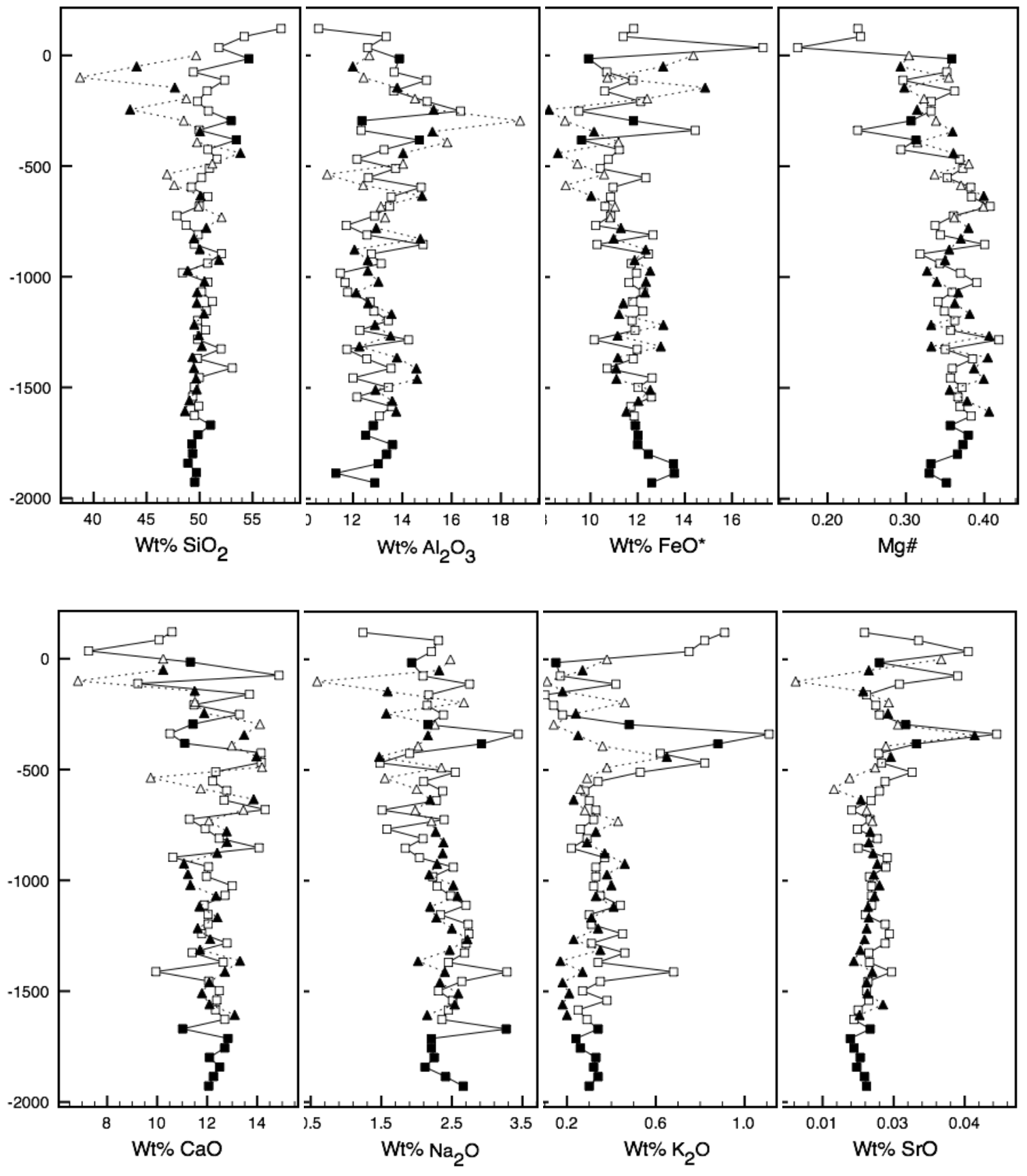


Fig. 4 Chemical composition of whole rock (cuttings) from wells HE-50 (triangle) and HE-51 (squares) in Hellisheiði Geothermal Field. Filled objects are isotope samples.

3.2 Microprobe analysis

Epidote crystals selected for the present study of strontium isotopes are either infilling of pores and fractures or epidote crystals replacing original minerals, mostly plagioclase. In samples used for the microprobe analyses the associated alteration minerals were not separated from the epidote but analyzed simultaneously and listed in appendix II.

Table 3 Representative epidote analyses from Hellisheiði Geothermal Field

Well	HE-50	HE-50	HE-50	HE-51	HE-51	HE-51	HE-51
Depth	-1118	-1118	-1118	-1756	-1756	-1756	-1756
SiO ₂	36.92	37.60	37.74	37.30	38.42	38.28	37.24
TiO ₂	0.14	0.10	0.01	0.04	0.09	0.05	0.19
Al ₂ O ₃	22.34	22.83	24.04	26.56	26.90	27.03	23.81
Fe ₂ O ₃	14.23	13.86	11.76	10.02	8.99	9.06	11.98
CaO	23.24	23.36	23.27	22.80	22.92	23.00	23.16
SrO	0.06	0.06	0.09	0.17	0.43	0.50	0.19
Total	96.94	97.82	96.92	96.89	97.76	97.92	96.56
Si	2.986	3.005	3.019	2.961	3.011	2.998	2.997
Al	0.009	0.006	0.001	0.002	0.005	0.003	0.012
Ti	2.130	2.150	2.266	2.485	2.485	2.495	2.258
Fe ³⁺	0.866	0.833	0.708	0.598	0.530	0.534	0.726
Ca	2.014	2.000	1.995	1.939	1.925	1.931	1.997
Sr	0.003	0.003	0.004	0.008	0.020	0.023	0.009
Total	8.007	7.997	7.993	7.994	7.976	7.984	7.999
Ps	28.913	27.931	23.805	19.407	17.588	17.624	24.319

Representative microprobe analyses of epidote are given in Table 3. The major compositional variation is in the octahedral sites substitution of Fe³⁺ and Al³⁺. Observed compositional range is X_{ps} 0.16 - 0.32. Earlier observations on samples from Nesjavellir show a wider compositional range (X_{ps} 0.10 - 0.41) (Hreggvidsdottir, 1987) and compositional range of epidotes from Krafla and Reykjanes is (X_{ps} 0.18-0.32) and (0.17 - 0.48) respectively (Freedman et al., 2009; Sveinbjornsdottir, 1991). Strontium concentration in the analyzed epidotes ranges from 0.03 to 0.5 Wt% SrO.

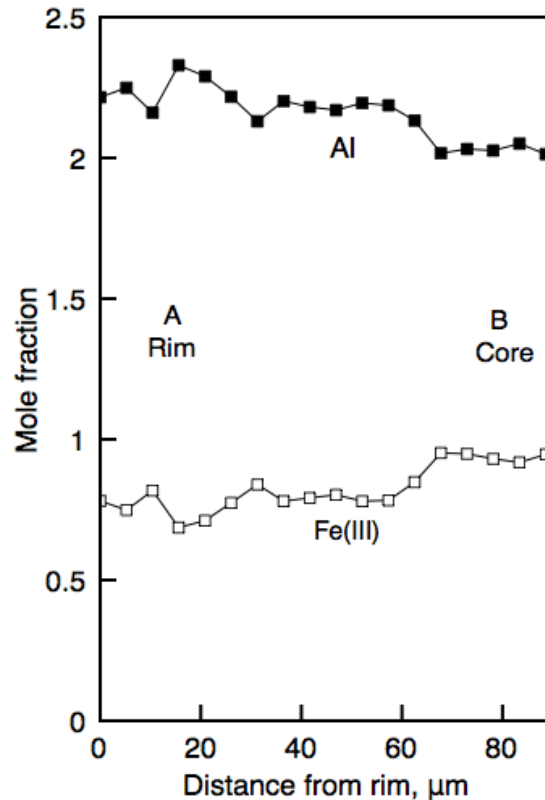


Fig. 5 Section A-B shows the traverse of the probe scan. The epidote column shows Fe(III) rich cores and Al-rich rims. Epidote from vein filling at -1076 m b.s.l.

A slight decrease in iron with depth is observed and similar slight decrease has been observed in the Reykjanes geothermal field (Freedman et al., 2009; Marks et al., 2010). Epidotes from both wells are commonly zoned with Fe-rich core and Al enrichment towards the rims (fig. 5). The minor element Ti follows iron in core of the crystal and is probably a far better indicator of zoning than iron. Strontium enrichment towards the rim is shown in fig. 6. Although irregular zoning in epidotes may be apparent on a polished surface the reason is in most cases that early epidote crystals growing in cavities form fan shaped needle aggregates where each needle is compositionally zoned. A polished surface of such aggregates may, depending on cutting angle, appear as irregular zoning within a large crystal.

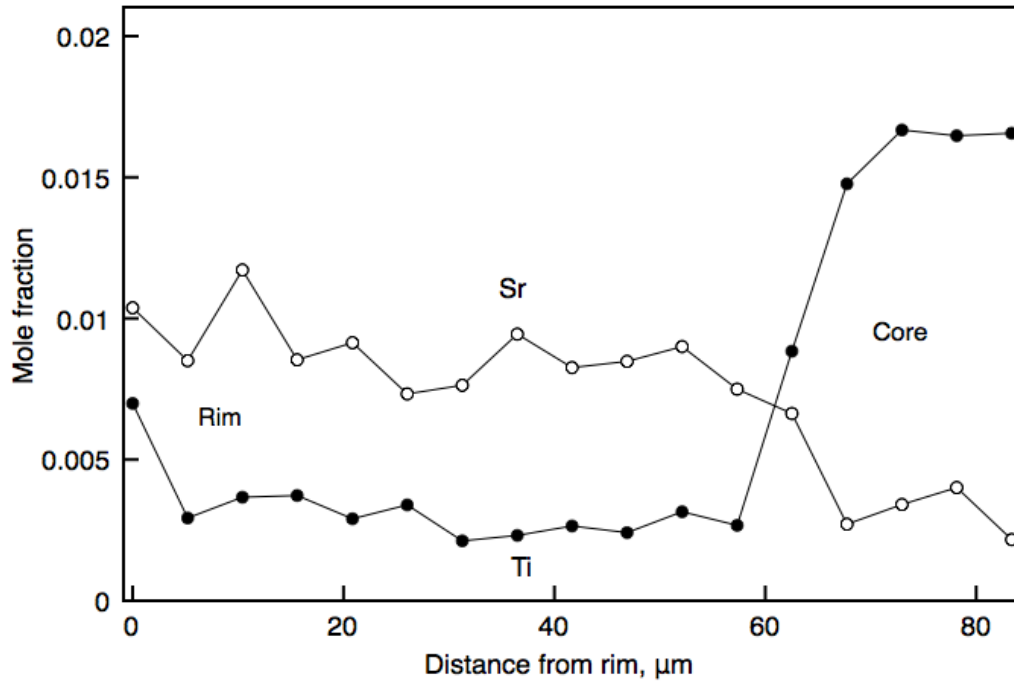


Fig. 6 Section shows the traverse of the probe scan. The epidote column show Ti rich cores and Sr-rich rims. Epidote from vein filling at -1076 m b.s.l.

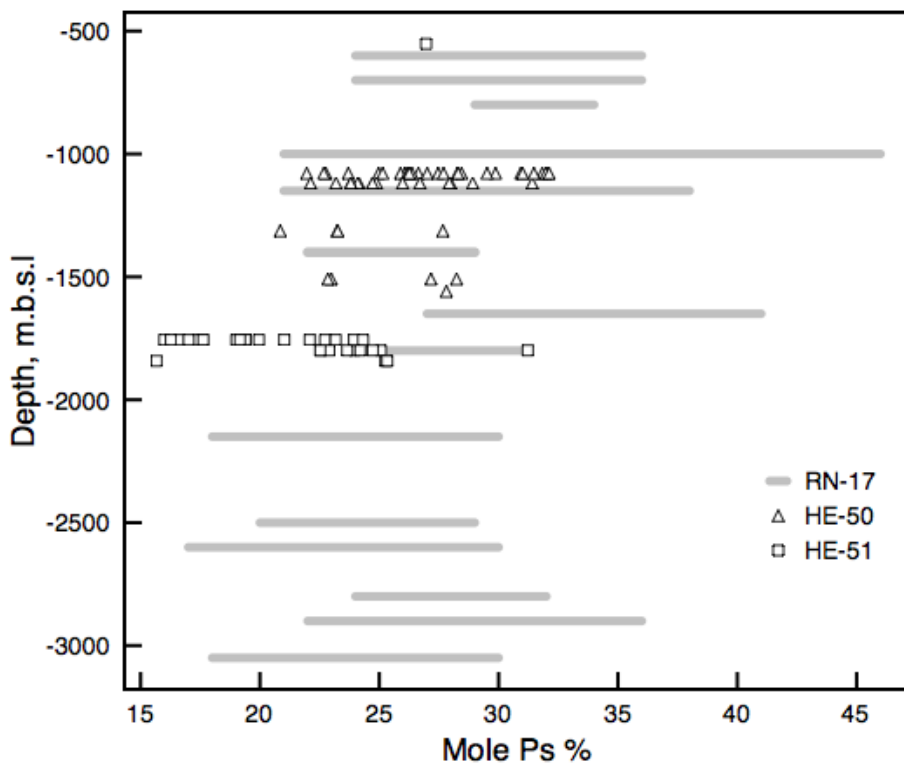


Fig. 7 Epidote Ps ($n_{Fe} / (n_{Al} + n_{Fe})$) plotted against depth from wells HE-50 and HE-51 in Hellisheiði geothermal system. Gray lines indicate RN-17 from Reykjanes Geothermal Field (Freedman et al., 2009) (Explanation for Ps is given on page 19)

3.3 Strontium isotopes analyses

There is a significant and measurable difference between the $^{87}\text{Sr}/^{86}\text{Sr}$ ratio of the original source rocks of the aquifer systems, about 0.70314, and the sea-water-derived meteoric water with 0.70916 that feeds the geothermal systems. $^{87}\text{Sr}/^{86}\text{Sr}$ measurements were made on the separated clay fractions, with a range from 0.703116 to 0.703875 (Table 4), and on hand-picked epidote that range from 0.703104 to 0.70336 (Table 5). This range, which far exceeds that of igneous rocks in Iceland, is illustrated in Fig. 13 and clearly shows the sea-water impact on the Sr budget of the reservoir rocks.

Table 4 Strontium isotope ratios in clay fraction from HE-50 and HE-51

Sample	Depth (m b.s.l)	$^{87}\text{Sr}/^{86}\text{Sr}$	$\pm 2\sigma$
HE-50 152	152	0.703140	0.000058
HE-50-50	-50	0.703719	0.000033
HE-50-145	-145	0.703875	0.000060
HE-50-247	-247	0.703370	0.000046
HE-50-344	-344	0.706182	0.000035
HE-50-441	-441	0.703277	0.000059
HE-50-634	-634	0.703184	0.000062
HE-50-827	-827	0.703158	0.000067
HE-50-924	-924	0.703149	0.000063
HE-50-1021	-1021	0.703397	0.000046
HE-50-1079	-1079	0.703214	0.000050
HE-50-1118	-1118	0.703152	0.000029
HE-50-1167	-1167	0.703152	0.000050
HE-50-1216	-1216	0.703231	0.000045
HE-50-1265	-1265	0.703116	0.000041
HE-50-1313	-1313	0.703195	0.000045
HE-50-1363	-1363	0.703156	0.000037
HE-50-1412	-1412	0.703167	0.000040
HE-50-1460	-1460	0.703139	0.000031
HE-50-1509	-1509	0.703171	0.000041
HE-50-1559	-1559	0.703219	0.000040
HE-50-1607	-1607	0.703165	0.000033
HE-51-15	-15	0.703603	0.000033
HE-51-295	-295	0.703521	0.000032
HE-51-382	-382	0.703613	0.000052
HE-51-1670	-1670	0.703183	0.000054
HE-51-1713	-1713	0.703210	0.000051
HE-51-1713	-1713	0.703152	0.000053
HE-51-1756	-1756	0.703127	0.000067
HE-51-1799	-1799	0.703185	0.000037
HE-51-1885	-1885	0.703187	0.000048
HE-51-1928	-1928	0.703169	0.000206

Samples of geothermal fluid were not available from drillholes HE-50 and HE-51 but samples from drillholes close to HE-50 (HE-12, 17 and 18) were collected and analyzed. In addition, other fluid samples were collected and measured. The $^{87}\text{Sr}/^{86}\text{Sr}$ isotopic ratios of

the eight geothermal water samples are listed in Table 6 and locations showed on Fig 1. The $^{87}\text{Sr}/^{86}\text{Sr}$ range in the water samples is 0.703140-0.73875, similar to that of the clay fraction. Each fluid sample represents the integrated mixture of all the aquifers in the respective drillholes.

Table 5 Strontium isotope ratios in epidote from HE-50 and HE-51

Sample	Depth (m.b.s.l)	$^{87}\text{Sr}/^{86}\text{Sr}$	$\pm 2\sigma$
HE-50-779	-779	0.703360	0.000047
HE-50-876	-876	0.703233	0.000038
HE-50-924	-924	0.703146	0.000036
HE-50-972	-972	0.703238	0.000042
HE-50-1021	-1021	0.703202	0.000039
HE-50-1079	-1079	0.703254	0.000025
HE-50-1118	-1118	0.703242	0.000055
HE-50-1167	-1167	0.703169	0.000007
HE-50-1216	-1216	0.703189	0.000038
HE-50-1265	-1265	0.703165	0.000033
HE-50-1313	-1313	0.703215	0.000024
HE-50-1363	-1363	0.703179	0.000054
HE-50-1412	-1412	0.703319	0.000056
HE-50-1460	-1460	0.703277	0.000031
HE-50-1509	-1509	0.703211	0.000024
HE-50-1559	-1559	0.703104	0.000036
HE-51-295	-295	0.703234	0.000038
HE-51-382	-382	0.703411	0.000072
HE-51-552	-552	0.703205	0.000070
HE-51-1670	-1670	0.703128	0.000050
HE-51-1713	-1713	0.703227	0.000031
HE-51-1756	-1756	0.703214	0.000015
HE-51-1842	-1842	0.703094	0.000044
HE-51-1885	-1885	0.703202	0.000044

Table 6 Strontium isotope ratios in geothermal water from Hellisheiði Geothermal Field

Sample	Well	$^{87}\text{Sr}/^{86}\text{Sr}$	$\pm 2\sigma$
Water_1	HE-6	0.703875	0.000035
Water_2	HE-11	0.703423	0.000093
Water_3	HE-12	0.703187	0.000052
Water_4	HE-17	0.703397	0.000069
Water_5	HE-18	0.703219	0.000090
Water_6	HE-30	0.703140	0.000059
Water_7	HE-46	0.703149	0.000044
Water_8	HE-47	0.703158	0.000065

4 Discussion

4.1 Formation and paragenesis of epidote

Epidote is one of the main index minerals for the zoning of geothermal alteration and it has a detectable (with the microprobe) content of Sr which also is high enough for $^{87}\text{Sr}/^{86}\text{Sr}$ ratio measurements. An outstanding feature of hydrothermally formed epidote in Icelandic geothermal systems is the ubiquitous zoning with Fe richer cores and Al richer rims fig. 5. This is accompanied by lower Sr concentration in the cores and enriched in the rims and with the reverse for Ti (fig. 6).

Formula for epidote is $\text{Ca}_2\text{Fe}_x\text{Al}_{3-x}\text{Si}_3\text{O}_{12}(\text{OH})$ and major element variation is in the $\text{Fe}^{3+}/\text{Al}^{3+}$ ratio in octahedral sites. There are three octahedral sites M1, M2 and M3 in monoclinic epidote, Fe(III) substitutes for Al in both M1 and M3 sites with M3 being the preferred site for Fe(III) (Arnason, 1993). The M2 site only contains Al at low hydrothermal temperature but at higher temperature Fe(III) enters the M2 site. Temperatures in the Hengill system are likely to be too low for this to have a significant effect (Freedman et al., 2009). Clinozoisite is the $\text{Ca}_2\text{Al}_3\text{Si}_3\text{O}_{12}(\text{OH})$ end member but pistacite, the theoretical Fe-epidote end member $\text{Ca}_2\text{Fe}_3\text{Si}_3\text{O}_{12}(\text{OH})$ does not occur in nature. The composition of the epidotes is reported as mole fraction of pistacite. The mole fraction $n_{\text{Fe}} / (n_{\text{Fe}} + n_{\text{Al}})$, where n_{Fe} and n_{Al} represent the mole atoms in each formula unit, is used as X_{ps} . Strontium is important minor element in epidote and previous analysis of Icelandic epidotes show that the SrO content ranges from 0.016 - 0.90 % with average 0.23% SrO (Exley, 1982). In Hengill the SrO increases towards the rims possibly reflecting extendent breakdown of plagioclase.

The epidotes found among hydrothermal alteration minerals in Iceland are yellowish to green xenoblastic crystals <0.8 mm. Epidote at early stages of growth often occurs as fan-shaped aggregates of small columnar crystals (25-250 micrometer) that generally form the core of larger crystals. Epidote in the chlorite epidote zone and the epidote-actionolite zone also appears as compact large crystals replacing plagioclase (Lonker et al., 1993). Epidote is widely distributed throughout wells HE-50 and HE-51 and occurs as a vein- or amygdaloidal mineral forming in open space as well as replacement crystals within plagioclase pseudomorphs (Fig. 11).

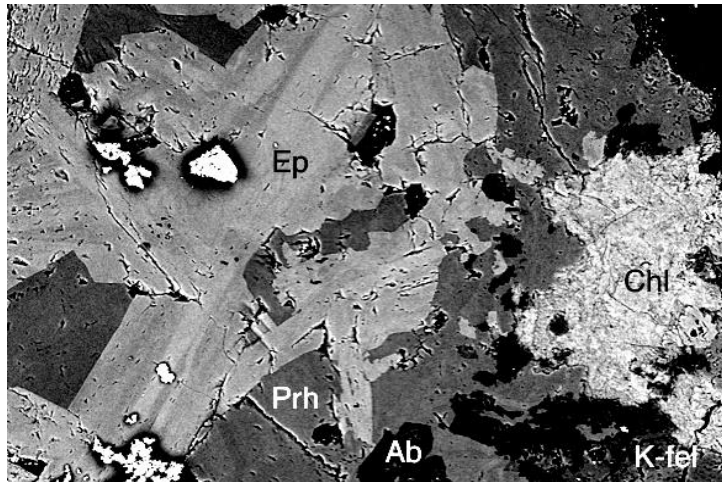


Fig. 8 SEM microphotograph, backscatter image, baseline length 350 μm . Some of the typical features of hydrothermal epidote paragenesis are displayed in the figure. The light core of the epidote needles represent iron rich composition while the darker margins are iron poor. Prehnite is in a close relation to the epidote and both phases are embedded in a matrix of clay minerals where the ever-present hydrothermal feldspars are also present. Note the dendritic titanomagnetite cluster in the lower left and the titanomagnetite inclusion in the epidote. Sample from HE-50 at -1713 m b.s.l.

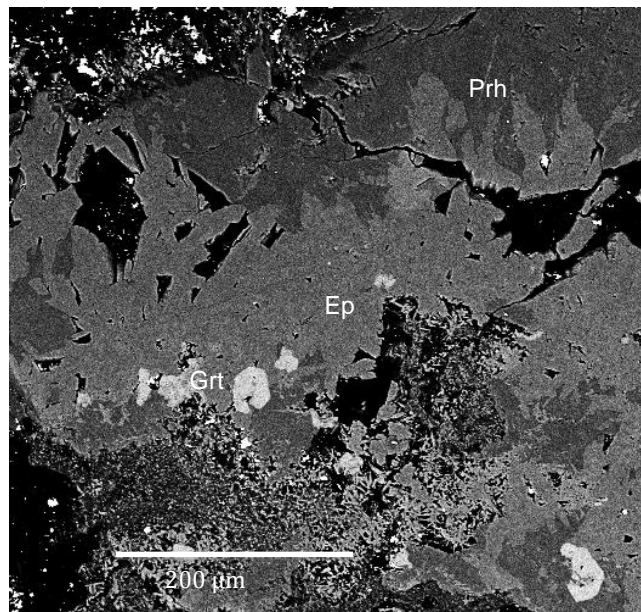


Fig. 9 Epidote-Prehnite vein with andradite garnet, HE-50 at -827 m b.s.l.

Epidote is associated with wairakite, prehnite, andradite, chlorite, quartz, calcite, actinolite, titanite, wollastonite, plagioclase, K-feldspar and oxides at different state of oxidation and exolution. (Fig 8).

Epidote first appears in active geothermal systems in temperature range from 200° to 250° and becomes abundant above 260°C. Within the upper chlorite-epidote zone Fe-rich epidote occurs with hematite, wairakite and andradite. This scenario has been related to highly oxidized environments (Liou, 1993).

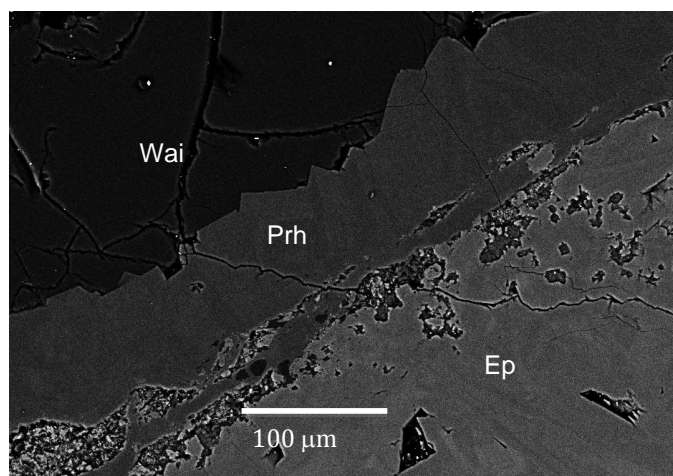


Fig. 10 SEM microphotograph, backscatter image. Wairakite (upper left) is replaced by prehnite with well evolved crystal phases. Epidote grows into the prehnite mass along a reaction zone, HE-51 at -1670 m b.s.l.

Within the mid- to lower chlorite-epidote alteration zone, epidote frequently appears with prehnite, wairakite and andradite, sometimes as inclusion in epidote as shown in fig 9. There is no doubt that andradite predates epidote in the alteration process and also that prehnite is often formed before epidote. All three phases occur together throughout the chlorite-epidote alteration zone. Wairakite, prehnite epidote paragenesis is displayed in fig. 10 where prehnite is evolving into a wairakite domain and epidote is replacing the prehnite.

In the epidote-actionolite zone the extent of alteration increases and igneous plagioclase and clinopyroxene are consumed by replacement minerals (Helgadottir, 2011) (Fig 12). In the 1990 m deep IRDP drillhole in the Tertiary of East Iceland, Exley (1982) reported analyses of 447 epidote crystals from the entire core. He observed that most of the hydrothermally formed epidotes have Fe-rich core and evolve towards Al-rich composition. Exley (1982) reported convincing evidence that the chemical variation of each single epidote is similar to the variation within a single lava flow and, moreover, identical with the variation for the entire IRDP- drill hole. This evidence rules out that fluctuations in CO₂ can control the repeated zoning of epidote within kilometers deep crustal sections. The pieces of information represented above illustrate that epidote forms initially within well defined paragenesis with two other Fe(III) silicates; prehnite and andradite.

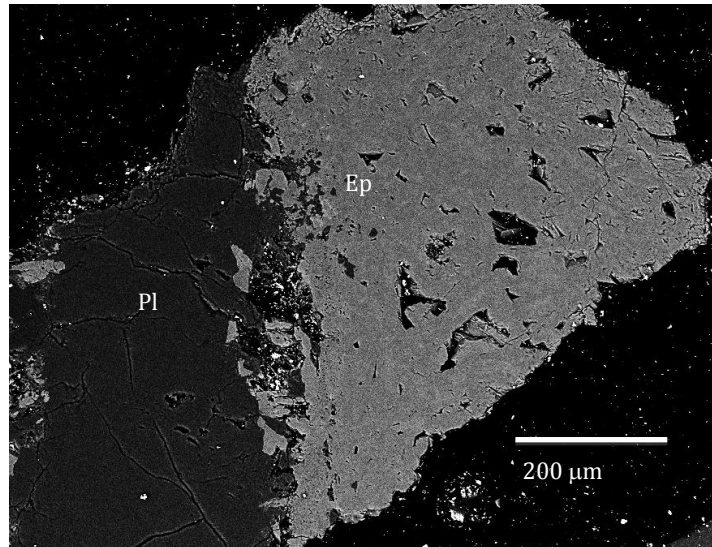


Fig. 11 Primary plagioclase replaced by epidote in HE-51 at -1885 m b.s.l. SEM microphotograph, backscatter image, baseline length 550 μm . Virtually unzoned epidote (upper right) replacing plagioclase. The reaction rim has to be fed with Fe(III) from the fluid.

The formation of the alteration phases is here interpreted as an interplay of the changing mineralogy and this in turn bears on the severe oxidation of the subsiding strata, yielding increasing Fe(III) as observed for the Hellisheiði geothermal field (Snæbjörnsdóttir, 2011). A search for an explanation for the repeated and ever-present zoning of epidote boils down to the question of what process within the chlorite-epidote facies takes over the control of Fe(III) and restricts its availability to epidote at the later stages of growth. It is difficult to postulate changes in the availability of Al since the entire system is equilibrated with albite and K-fsp as is observed and confirmed by the general validity of alkali thermometry in geothermal systems. A remaining variable which here is suggested as the controlling factor is the stability of hematite and its control of restricting the availability of Fe(III) in the fluid. Igneous FeTi-oxides in geothermal systems undergo systematic oxidation-dissolution within the chlorite epidote zone (Gunnarsdóttir, 2012; Steinthorsson & Sveinbjörnsdóttir, 1981). This may, indeed, explain the compositional zoning of epidotes. When the dissolution of ilmenite sets in, titanite and brookite appear in the mineral assemblage. This marks the beginning of Ti-mobility, as indicated by increased Ti in epidote, and changing Fe(III) mobility. Titanomagnetite transforms to metastable maghemite upon oxidation but in the chlorite epidote zone it is finally transformed to stable pure hematite. It is suggested here that the compositional zoning of Fe and Ti in epidote, observed in almost every crystal and every lava throughout kilometers of crustal sections is controlled by the appearance of hematite as the stable Fe(III) controlling mineral and restricting the Fe(III) availability.

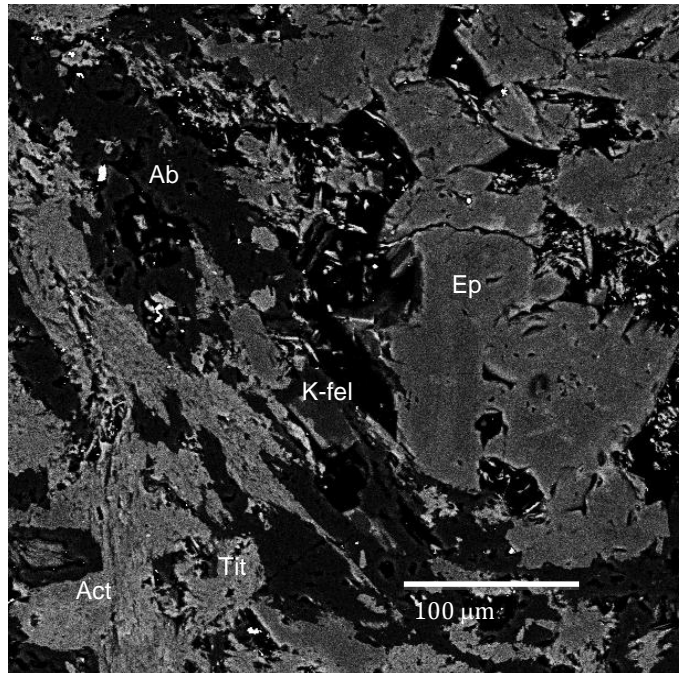


Fig. 12 Epidote associated with actinolite, albite, K-feldspar and titanite from -1559 m b.s.l from HE-50. SEM microphotograph, backscatter image. Typical paragenesis of epidote in the epidote actinolite facies. Actinolite grows along veins while the matrix is rich in albite with occasional K-fel. The hydrothermal alkali feldspars are all that remain of the igneous plagioclase that was replaced by epidote.

These conditions may, indeed, be changing during fluctuations in redox potential due to H_2S and CO_2 equilibrium of the geothermal fluid. A supporting evidence for this hypothesis is the more homogeneous iron poor composition of epidote that replaces plagioclase in the epidote-actinolite zone. Here, the minor compositional differences may be oscillatory or absent and the effect of variation in P may well apply. Moreover, the replacement epidotes are also markedly lower in Fe as compared with the cores of the early phases.

In summary, the earliest Fe-rich cores of epidote may be formed from the common intermediate hydroxy-anorthite component derived from plagioclase, andradite and Fe(III) derived from the oxidation of titanomagnetite according to Donohue and Essene (2000). Epidote replacement in altered gabbro in Southeast Iceland is almost homogeneous due to uniform alteration environment (Guðmundsson, 2009)

One suggested explanation for the zoning in epidote may be controlled by increased P_{CO_2} where conditions are near isothermal (Freedman et al., 2009). Intrusion activity caused by rise in the CO_2 content in the hydrothermal fluids. This in turn lowers its pH and affects and the speciation of Fe^{3+} and Al^{3+} . At near neutral pH the predominant species of Fe^{3+} and Al^{3+} are $Fe(OH)_3^0$ and $Al(OH)_4^-$, so under these conditions iron in epidote will decrease with decreasing pH (Bird & Spieler, 2004). By anorthite hydrolysis OH^- is consumed to form $Al(OH)_4^-$ which lowers the pH. The effects of changing P_{CO_2} can however, not be applied at temperature exceeding the solubility field for calcite, since calcite is involved in the reaction considered and calcite is absent in the epidote-actinolite zone of the well HE-50.

The general interplay between the different minerals during alteration can be described by a few relatively simple equations listed below.

Equation 1



After prolonged oxidation leading to hematite, according to experiments by (Moody, Meyer, & Jenkins, 1983), the epidote formation may continue according to:

Equation 2



The classical equation (Liou 1993; Liou et al., 1983) for epidote formation:

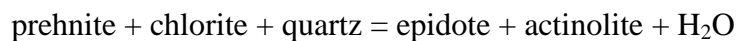
Equation 3



may proceed simultaneously and there is no way to distinguish between the two alternatives in the cuttings from wells HE-50 and HE-51 due to the complexity of the mineral assemblage.

In the epidote-actinolite zone where dehydration and breakdown of chlorite may lead to the reaction

Equation 4



which describes a realistic paragenesis of epidote as it appears in the core samples from wells HE-50 and HE-51. Taken together, these equations involve dehydration of the alteration mineral assemblage, a result that conforms to recent analysis of the water content of alteration minerals from the Hellisheiði geothermal field (Snæbjörnsdóttir, 2011). Finally, it is noted that the present suggestion for epidote paragenesis implies continued growth of epidote down the wells which conforms to the observed strontium isotope shift towards rock values with increasing depth.

The increased Sr content in the rims of the epidote most likely corresponds to extensive dissolution of plagioclase – the main source of Sr in the original minerals.

4.2 Strontium isotopes

The large and significant difference between $^{87}\text{Sr}/^{86}\text{Sr}$ in meteoric (sea water) and the original rock can be very useful in tracing the water-rock patterns in geothermal systems but it has to be kept in mind that the overwhelming source of Sr in the system, in terms of concentration, is in the rocks so large amount of water have to be circulated through the system to have marked effect. In the present work the $^{87}\text{Sr}/^{86}\text{Sr}$ ratio was measured in the clay fractions of the drill chips available throughout the depth range of both cores. In addition eight geothermal fluid samples from different parts of the Hengill geothermal system were analyzed. Unfortunately no samples were available from drillholes HE-50 and HE-51 but the results do throw light on some of the general characteristics of $^{87}\text{Sr}/^{86}\text{Sr}$ behavior in the geothermal fields.

4.2.1 $^{87}\text{Sr}/^{86}\text{Sr}$ in the drill cuttings.

The results are displayed in fig. 13 where $^{87}\text{Sr}/^{86}\text{Sr}$ for both the clay fraction and epidote for both drillholes are plotted versus depth and the main aquifers encountered during drilling are indicated. The values for the acid leached clay fraction range from 0.70311 - 0.70387 (Table 4). The high range is restricted to the shallow zeolite and chlorite zones where mainly clay fraction samples are available. In the chlorite-epidote alteration zone ratios are much more restricted with the average of 0.70319.

A reference line for $^{87}\text{Sr}/^{86}\text{Sr}$ value of 0.70314 is displayed in fig. 13. This is a value that appears to be most common in the volcanic centers in the Icelandic rift zones (Peate et al., 2009) and in Hengill (Magna et al., 2011). However, lower values are observed in olivine tholeiites down to as low as 0.70301 (Karl Gronvold per. com.) also shown on fig. 13. This is relevant as the deeper parts of the reservoir rocks are interpreted as lava flows that predate the beginning of the central volcano activity. This is in good accord with the lower $^{87}\text{Sr}/^{86}\text{Sr}$ ratios observed in the lower third of the drillhole cuttings.

In the upper part of the drillholes there is a significant isotope shift towards meteoric $^{87}\text{Sr}/^{86}\text{Sr}$ relative to that of the original source rocks - especially for the the clay fraction but less for the epidotes. This is also the level with most variable and higher Sr content fig. 4 . In the lower part of the drillholes there is a lesser shift towards meteoric water but as expected all the ratios are higher than the range of source rock values.

In drillhole HE-50 at three depth intervals in the epidote alteration zones, at 1150, 1400 and 1800m, the $^{87}\text{Sr}/^{86}\text{Sr}$ have distinctively higher isotopic ratios relative to the average values in the alteration minerals. These higher values are at fluid feed zones (Gunnarsdóttir et al., 2010) where the shift towards rain-strontium, indicating fluid values. These are the depth ranges where samples coincide with suggested feed zones.

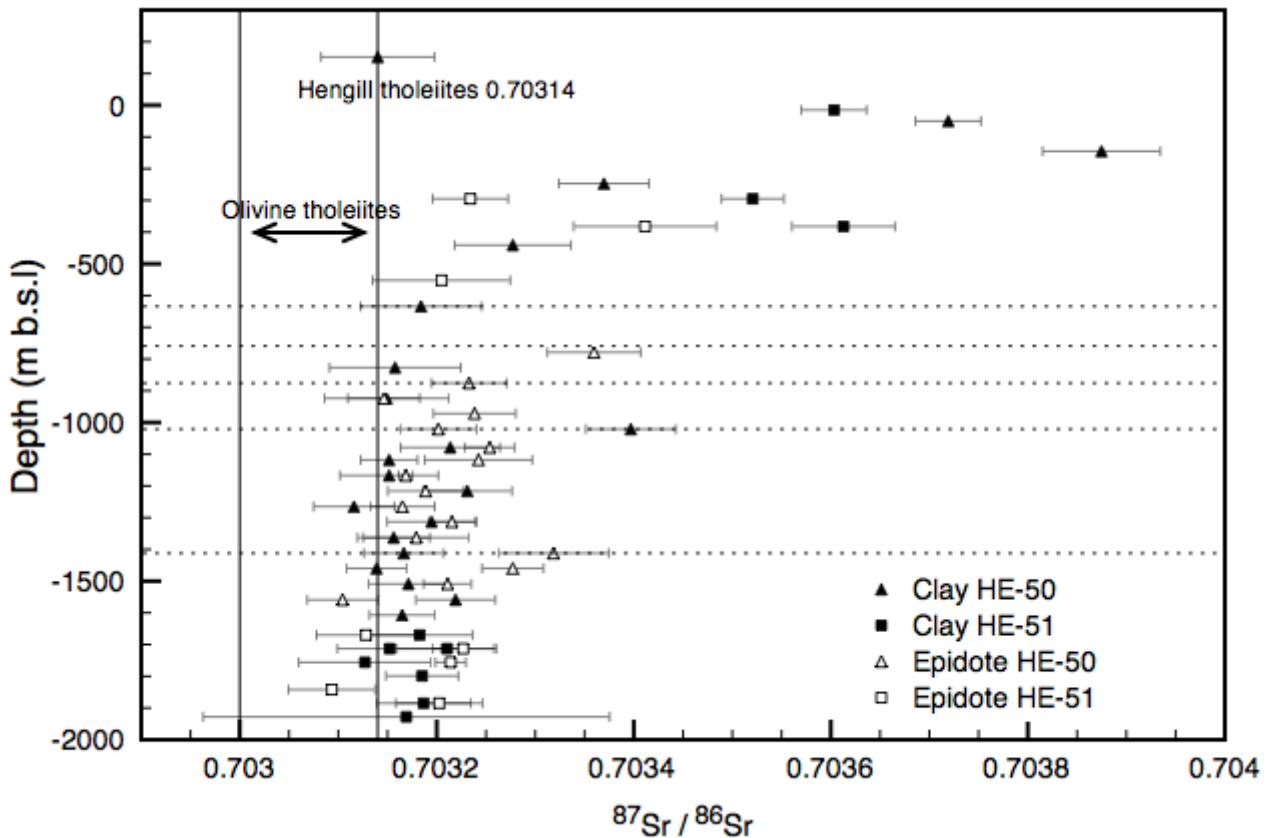


Fig. 13 Strontium isotope ratios plotted against depth in well HE-50 and HE-51. Dotted line are feed points

The overall pattern of the $^{87}\text{Sr}/^{86}\text{Sr}$ isotope shift in alteration minerals from the Hellisheiði Geothermal Field is that Sr from precipitation is collected by the earliest alteration minerals and continued alteration within the subsiding rock-pile and equilibration of Sr among the alteration phases dilutes the isotope shift with rock Sr. Still, the isotope shift is measureable down to the bottom of the wells.

The present results conform broadly to results from the meteoric water dominated Krafla geothermal field in North Iceland (Oskarsson, 2006). Strontium isotope ratios of geothermally-altered rock and geothermal fluids in the sea water dominated Reykjanes and Svartsengi (Elderfield & Greaves, 1981) give ratios 0.7038-0.7042 for the altered rock from Reykjanes and 0.7039-0.7041 for Svartsengi. It is evident that seawater dominated geothermal systems are displaying similar processes as observed in the present study but at much higher $^{87}\text{Sr}/^{86}\text{Sr}$ levels. These and more recent research on strontium isotopes in epidote and anhydrite from the seawater dominated Reykjanes geothermal field ((Marks et al., 2011; Marks et al., 2010; Raffone et al., 2010) confirm the earlier work but interestingly the epidote at the aquifers is also elevated to even higher ratios than the geothermal fluids. The recharge water is sea water with much higher Sr concentrations reflected in generally higher $^{87}\text{Sr}/^{86}\text{Sr}$ of the whole system

4.2.2 Geothermal fluid

Geothermal fluid samples were available for $^{87}\text{Sr}/^{86}\text{Sr}$ measurements from the Hellisheiði geothermal fields - but not including HE-50 and HE-51. The results are listed in Table 7

and the locations with directions of the drillholes are shown in Fig. 1. The results show a significant spread in $^{87}\text{Sr}/^{86}\text{Sr}$ ratios from 0.703140 - 0.70387 in the eight different wells. Four out of eight wells show significant levels of meteoric Sr (wells HE-6, HE-12, HE-17, and HE-18) but the other four show a strong $^{87}\text{Sr}/^{86}\text{Sr}$ isotope shift towards igneous rocks having values close to the assumed reservoir rock ratios.

Individual fluid samples represent the total outflow and can therefore be a mixture of water from many aquifers and different depths and temperatures but no attempt has been made here to estimate contributions from different aquifers. The different levels of $^{87}\text{Sr}/^{86}\text{Sr}$ in the water may thus be explained by equilibration with the rock with different degree of meteoric impact. It is evident from the mineral $^{87}\text{Sr}/^{86}\text{Sr}$ that the meteoric $^{87}\text{Sr}/^{86}\text{Sr}$ signal in the water will fade completely with depth being finally dominated the high amount of Sr in rocks as compared to the precipitation and the previous stripping of $^{87}\text{Sr}/^{86}\text{Sr}$ at the upper levels. Since the high $^{87}\text{Sr}/^{86}\text{Sr}$ signal is still present in some of the fluids, its relations to topography, hydrology and age of water may shed some light on the overall water-rock relations.

To a first approximation, the controlling factors of the fluid $^{87}\text{Sr}/^{86}\text{Sr}$ are likely to be the ratios of the aquifer rocks but the time duration of the water rock interaction may also in some cases be a controlling factor as indicated by the elevated $^{87}\text{Sr}/^{86}\text{Sr}$ in minerals close to the suggested aquifers.

In Fig 14 the $^{87}\text{Sr}/^{86}\text{Sr}$ ratios of the fluids are plotted “downstream” within the rift-zone in an attempt to connect the $^{87}\text{Sr}/^{86}\text{Sr}$ values of the water to the hydrological scenario of the Hellisheiði fields. In Fig. 1 the location of the wells are shown and their surface projection is shown as dotted lines. The position of the center of each well is then marked as the distance in fig. 14.

These results show that water of wells, furthest south relative to the Hengill volcanic center, the highest degree of equilibration with the rock.

One well at the western rift margin also shows $^{87}\text{Sr}/^{86}\text{Sr}$ ratio that indicates high degree of equilibration with the rock.

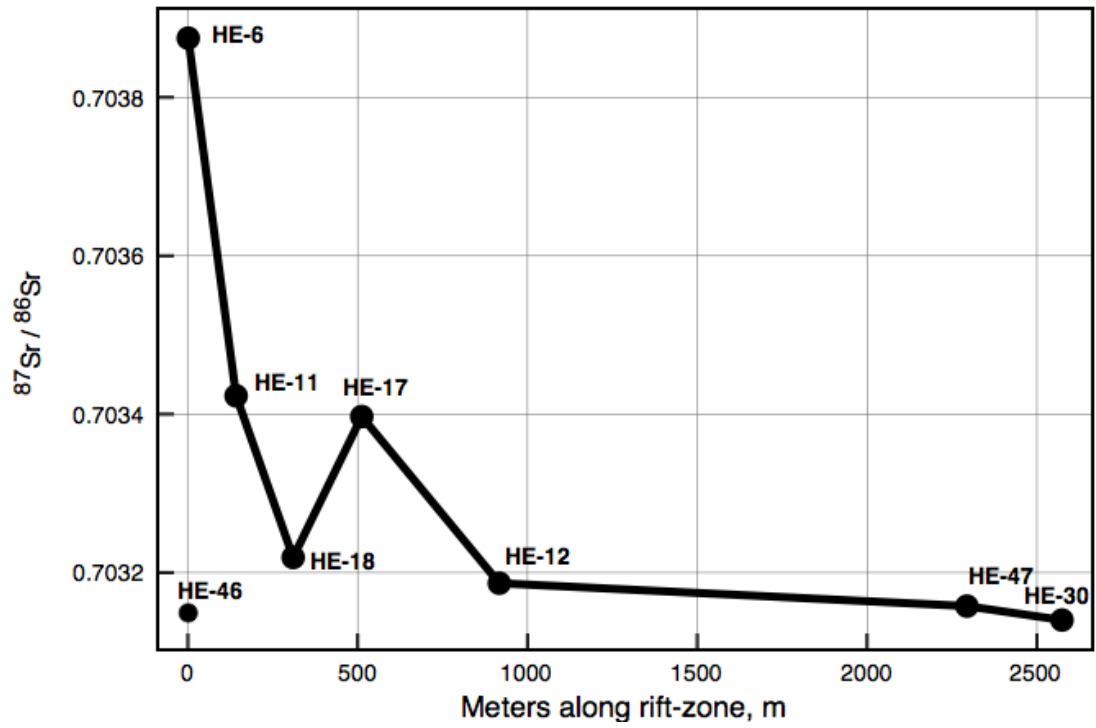


Fig. 14 Strontium isotope ratios in geothermal water plotted against distance in meters

5 Summary and conclusions

The basic reason for attempting to use $^{87}\text{Sr}/^{86}\text{Sr}$ to further understanding of the hydrology and water-rock interactions is the large difference in the $^{87}\text{Sr}/^{86}\text{Sr}$ ratio in sea-water-derived meteoric water (0.709) and the original rock ratios (about 0.70314). With the measurement precision (about 0.0004) relatively small interaction and mixing between the host rock and water is detectable. Concentration of Sr and its transfer mechanism is also an important consideration with the concentration difference between a kilo of source rock and a liter of meteoric water being around 100,000 fold. The transfer of Sr involves the breakdown of original rock (glass and crystals) and the recrystallization of old minerals and precipitation of new ones next to the original ones. The results from this study and other studies so far show that meteoric signal is detectable in many samples of alteration minerals and geothermal waters. In detail however it is the differences that may be of the greatest interest as they still reflect varying meteoric-water influence on different parts of the geothermal and hydrological systems.

The long-term exploration and exploitation of the Hengill geothermal systems has produced an extensive body of research papers and greatly increased understanding of these systems (Franzson et al., 2010; Franzson et al., 2005; Helgadóttir et al., 2010). But many fundamental questions remain unanswered and there are many aspects that complicate simple explanations and general models. This information has important bearing on the interpretation of the present results. When looking at the results and their interpretation it is important to remember that the borehole material used and water samples analyzed were selected based on sample availability at the time rather than overall strategy.

There are important changes in the nature of the original source rocks with depth. The upper five hundred meters of the rocks are dominated by hyaloclastites, often with only limited amount of phenocrysts and thus dominated by glass that alters relatively easily and is often totally altered. Below that are other five hundred meters of alternating layers of hyaloclastites and lava flows. But the bottom half of the holes are crystalline lava flows with increasing amount of crystalline intrusives (Helgadóttir et al., 2010). Both lava flows and intrusives have only minimal amount of glass and generally show less intensive alteration. There is a fundamental difference in the paths, on the one side, of hyaloclastites and lavas that all start at the surface and then subside to their present position and therefore go gradually through the alteration processes and, on the other side, of intrusives that are intruded into already-established alteration zones causing locally higher-temperature alteration that then retrogrades into the prevailing alteration. All this can affect the details of the chemical composition of the alteration products.

Another important factor affecting the alteration patterns and alteration history is the effect of glaciations which is reflected in the discrepancy between present-day thermal state of the reservoir formations and the temperature deduced from the alteration mineralogy and fluid inclusion studies that commonly shows significantly higher temperatures for the alteration. This is best explained by higher hydrostatic pressures and hence higher temperatures due to the ice burden during glaciations (Franzson et al., 2010). This could

then be further complicated by changes in the ice burden due to the large climate changes during the last glacial 150 thousand to 14 thousand years but with maximum ice thickness during the LGM (Last Glacial Maximum) around 22 thousand years ago. A further implication of the thick ice cover is possible changes in the hydrology due to effect on the downflow feed zones.

One noticeable feature reported on the Hengill area are present day reversed thermal gradients in many of the drillholes (Franzson et al., 2010; Helgadóttir et al., 2010). In HE-50 a maximum temperature of about 280°C is reached at about 1250 meters and a few hundred meters of slight cooling until previous temperature is reached again. An obvious question is whether this is a transient phenomenon and then if this is a part of a general recovery of deglaciation cooling and/or influenced by the general hydrological flow of Hengill. There appear to be two explanations for the reversed thermal gradients in the formation temperatures. The upper parts could be in the process of heating up due to upflow and then horizontal flow where the maximum temperatures are observed, or cooling below the maximum due to flow of colder water that is recharging the thermal system. Or a combination of both.

A final observation that may affect interpretation of the epidote and Sr-isotope data is the interpretation of the discrepancies between formation temperatures observed from temperature measurements in the drillholes and the temperature derived from the state of alteration. This indicates that zones close to the 2000 and 5000 year old eruptive fissure have formation temperatures higher than the alteration temperatures and thus may be in the process of heating up relative to surrounding zones that still preserve the glacial time thermal state. This pattern is thought to reflect changes in the thermal water flow most likely influenced by the Holocene tectonics and possible rifting events (Franzson et al., 2010).

The zoning of epidote grains as has been observed in other studies is confirmed in the present study as is the observation that the whole range observed in a system can be observed in a very limited depth range and even down to the single grain scale (Exley 1982; Freedman et al., 2009; Marks et al., 2010). The pattern is lower Al rims and higher Fe cores. It is argued here that this is most likely a reflection of the changing mineralogy during alteration of iron being depleted in the fluids due to hematite control reflecting increased oxidation with depth. The influence of plagioclase breakdown is also indicated by the increased Sr content of the epidotes in the rims accompanying the increased Al. The implication of this is that most of the Sr isotope signal in epidotes is obtained in the later and higher temperature stage of alteration.

The Sr-isotopic ratios of the epidote and clay fraction are fairly similar in $^{87}\text{Sr}/^{86}\text{Sr}$ and when both have been analyzed at the same depth there is not a significant difference between the two. The samples have $^{87}\text{Sr}/^{86}\text{Sr}$ ratios that range from the expected fresh rock values and to significantly higher values that are taken to reflect significant rain water strontium. A significant feature is the high values in the upper 600 meters – as this is above the main epidote zone, mainly the clay fraction is available but the one epidote sample found is also high. This indicates that most of the meteoric component is removed by the zeolite and clay fractions and therefore resides in the cap rocks of the geothermal system. This is also reflected in the Sr concentration profile for the whole rock drill chips – although some of the variation there is likely to reflect greater original rock variation after the onset of the Central Volcano activity.

In the lower part of the holes, ratios range from expected original rock value but many values have higher ratios so at some stage meteoric Sr has survived into the deeper parts in spite of the large concentration difference. All the lowest values are within the original rock values expected within the original reservoir rocks. A few ratios are significantly higher - for both epidote and clays - than the deep samples in general and these coincide with locations where the samples come from same level as where major aquifers have been located. The rate of the alteration processes is not known but the results suggest that the aquifers have persisted for some time. The isotopic ratios of the minerals could be minimum values for the water feeding the aquifers but the similarity with water samples from other holes suggest that these reflect actual aquifer water and a relatively fast water circulation. This in turn indicates that water-rock estimates applied for the system as a whole have to be treated with some care.

The eight water samples were collected at wellheads. Samples were not available from HE-50 and HE-51 so the samples collected and analyzed cover a much wider range within the Hellisheiði Geothermal Fields. Without much more detailed background information discussion and interpretation is very tentative but some interesting observations emerge and show that this is clearly a worthwhile avenue to pursue. Five of the samples have $^{87}\text{Sr}/^{86}\text{Sr}$ ratios that are close to the original rock values and no higher than most of the ratios observed for epidotes and clays in holes HE-50 and HE-51. Three of the water samples show significantly higher value with two, HE-11 and HE-17, within range of higher ratios associated with the main aquifers in HE-50 and HE-51. The highest $^{87}\text{Sr}/^{86}\text{Sr}$ ratio observed is in hole HE-6 similar to the highest ratio observed in clay fractions in the upper 500 meters of the HE-50 and 51 holes. There is no $^{87}\text{Sr}/^{86}\text{Sr}$ alteration mineral data for the actual holes sampled for water but closeness of HE-50 to these three high $^{87}\text{Sr}/^{86}\text{Sr}$ holes suggests similar $^{87}\text{Sr}/^{86}\text{Sr}$ pattern for the alteration minerals. The location of the three holes to the 5000 year old eruptive fissure and the zone where formation temperatures exceed the alteration temperatures and hence are in the process of warming up suggests that water flow rates through the system are relatively faster than elsewhere in Hellisheiði.

References

- Arnason, J. G., Bird D. K., Liou J. G. (1993). Variables Controlling Epidotes Composition in Hydrothermal and Low-Pressure Regional Metamorphic Rocks. *Abhandlungen der Geologischen Bundesanstalt*, 49, 17-25.
- Bird, D. K., & Spieler, A. R. (2004). Epidote in Geothermal Systems. *Reviews in Mineralogy and Geochemistry*, 56(1), 235-300. doi: 10.2138/gsrng.56.1.235
- Coombs, D. S., Kawachi, Y., Houghton, B. F., Hyden, G., Pringle, I. J., & Williams, J. G. (1977). Andradite and Andradite-Grossular Solid-Solutions in Very Low-Grade Regionally Metamorphosed Rocks in Southern New-Zealand. *Contributions to Mineralogy and Petrology*, 63(3), 229-246.
- Donohue, C. L., & Essene, E. J. (2000). An oxygen barometer with the assemblage garnet-epidote. *Earth and Planetary Science Letters*, 181(3), 459-472.
- Elderfield, H., & Greaves, M. J. (1981). Strontium Isotope Geochemistry of Icelandic Geothermal Systems and Implications for Sea-Water Chemistry. *Geochimica Et Cosmochimica Acta*, 45(11), 2201-2212.
- Exley, R. A. (1982). Electron Micro-Probe Studies of Iceland-Research-Drilling-Project High-Temperature Hydrothermal Mineral Geochemistry. *Journal of Geophysical Research*, 87(Nb8), 6547-6557.
- Franzson, H. (1998). *Reservoir geology of the Nesjavellir high-temperature field in SWIceland*. Proceedings of the 19th Annual PNOC-EDC Geothermal Conference, Manila, Philippines, 5-6th 1998, 13-20.
- Franzson, H., Gunnlaugsson, E., Árnason, K., Sæmundsson, K., Steingrímsson, B., Harðarson, B. . (2010). *The Hengill Geothermal System, Conceptual Model and Thermal Evolution*. Paper presented at the World Geothermal Congress, Bali.
- Franzson, H., Kristján, B. R., Gunnarsson, G., Björnsson, G., Hjartarson, A., Steingrímsson, B., . . . Gíslason, G. (2005). *The Hengill-Hellisheiði Geothermal Field. Development of a Conceptual Geothermal Model*. Paper presented at the World Geothermal Congress, Antalya.
- Freedman, A. J. E., Bird, D. K., Arnorsson, S., Fridriksson, T., Elders, W. A., & Fridleifsson, G. O. (2009). Hydrothermal Minerals Record CO(2) Partial Pressures in the Reykjanes Geothermal System, Iceland. *American Journal of Science*, 309(9), 788-833. doi: Doi 10.2475/09.2009.02
- Fridleifsson, G. O. (1991). Hydrothermal system and associated alteration in Iceland (Vol. 277, pp. 83-89).
- Fridleifsson, G. O., & Elders, W. A. (2005). The Iceland Deep Drilling Project: a search for deep unconventional geothermal resources. *Geothermics*, 34(3), 269-285. doi: Doi 10.1016/J.Geothermics.2004.11.004
- Grapes, R. H., and Hoskin, W. O., 2004, Epidote Group Minerals in Low–Medium Pressure Metamorphic Terranes, *Reviews in Mineralogy & Geochemistry*, Vol. 56, pp. 301-345.

- Guðmundsson S. (2009). *Ummyndun í gabbroinnskotum á Suðausturlandi*. (B.Sc.), University of Iceland, Reykjavík. Retrieved from [http://www.vegagerdin.is/vefur2.nsf/Files/Ummyndun_gabbroinnskot_Sudausturl/\\$file/Ummyndun_gabbr%C3%B3innskot_Sudausturl.pdf](http://www.vegagerdin.is/vefur2.nsf/Files/Ummyndun_gabbroinnskot_Sudausturl/$file/Ummyndun_gabbr%C3%B3innskot_Sudausturl.pdf)
- Gunnarsdóttir, S. H. (2012). *Jarðfræði og ummyndun í nágrenni Reykjafells á Hellisheiði*. (Master), University of Iceland, Reykjavík. Retrieved from <http://hdl.handle.net/1946/10818>
- Gunnarsdóttir, S. H., Guðfinnsson, G. H., & Gunnarsson, H. S. (2010a). *Hellisheiði - Hola HE-50 3. áfangi*. In ÍSOR-2010/084 (Ed.). Reykjavík: ISOR.
- Gunnarsdóttir, S. H., Guðfinnsson, G. H., & Gunnarsson, H. S. (2010b). *Hellisheiði - Hola HE-50. Forborun, 1. og 2. áfangi*. In ÍSOR-2010/083 (Ed.). Reykjavík: ISOR.
- Hansteen, T. H. (1991). Multistage Evolution of the Picritic Maelifell Rocks, Sw Iceland - Constraints from Mineralogy and Inclusions of Glass and Fluid in Olivine. *Contributions to Mineralogy and Petrology*, 109(2), 225-239
- Helgadóttir, H. M., Snæbjörndóttir, S. Ó., Níelsson, S., Gunnarsdóttir, S. H., Mattíasdóttir, T., Harðarson, B., Einarsson, G. M., Franzson, H. (2010). *Geology and Hydrothermal Alteration in the Reservoir of the Hellisheiði High Temperature System, SW-Iceland*. Paper presented at the World Geothermal Congress, Bali.
- Hreggviðsdóttir H. (1987). *The greenschist to amphibolite facies transition in the Nesjavellir hydrothermal system*. (MSc), Stanford University, Stanford, California.
- Humphris, S. E., & Thompson, G. (1978). Hydrothermal Alteration of Oceanic Basalts by Seawater. *Geochimica Et Cosmochimica Acta*, 42(1), 107-125.
- Liou, J. G., Kim, H. S., Maruyama, S., 1983, Prehnite – Epidote Equilibria and their Petrologic Applications, *J. Petrol*, 24, 321-342.
- Kristmannsdóttir, H., 1979. *Alteration of basaltic rocks by hydrothermal activity at 100-300°C*. International Clay conference 1978. Ed.: Mortland and Farmer. Elsevier, Amsterdam, 277-288.
- Liou, J. G. (1993). Stabilities of Natural Epidotes. *Abhandlungen der Geologischen Bundesanstalt*, 49, 7-16.
- Lonker, S. W., Franzson, H., & Kristmannsdóttir, H. (1993). Mineral-Fluid Interactions in the Reykjanes and Svartsengi Geothermal Systems, Iceland. *American Journal of Science*, 293(7), 605-670.
- Níelsson, S. (2011). *Jarðfræði og ummyndun í jarðhitakerfinu við Hverahlíð á Hellisheiði*. (Master), University of Iceland, Reykjavík. Retrieved from <http://hdl.handle.net/1946/9894>
- Magna, T., Wiechert, U., Stuart, F. M., Halliday, A. N., & Harrison, D. (2011). Combined Li-He isotopes in Iceland and Jan Mayen basalts and constraints on the nature of the North Atlantic mantle. *Geochimica Et Cosmochimica Acta*, 75(3), 922-936. doi: Doi 10.1016/J.Gca.2010.11.007
- Marks, N., Schiffman, P., Zierenberg, R. A., Frannon, H., & Fridleifsson, G. O. (2010). Hydrothermal alteration in the Reykjanes geothermal system: Insights from Iceland deep drilling

- program well RN-17. *Journal of Volcanology and Geothermal Research*, 189(1-2), 172-190. doi: Doi 10.1016/J.Jvolgeores.2009.10.018
- Marks, N., Zierenberg, R., Elders, W. A., Fridleifsson, G. O., & Franzson, H. (2010, 25-29 April). *Isotopic Evidence of Hydrothermal Exchange and Seawater Ingress from Alteration Minerals in the Reykjanes Geothermal System: Results from the IDDP*. Paper presented at the World Geothermal Congress, Bali, Indonesia.
- Mattíasdóttir, T. & Ingólfsson, H. (2010a). *Hellisheiði - Hola HE-51 3. áfangi*. In ÍSOR-2010/109 (Ed.). Reykjavík: ISOR.
- Mattíasdóttir, T. & Ingólfsson, H. (2010b). *Hellisheiði - Hola HE-51 Forborun 1. og 2. áfangi*. In ÍSOR-2010/108 (Ed.). Reykjavík: ISOR.
- Marks, N., Zierenberg, R. A., & Schiffman, P. (2011). *Strontium and oxygen isotopic profiles through 3 km of hydrothermally altered oceanic crust in the Reykjanes Geothermal System, Iceland*. In press.
- Moody, J. B., Meyer, D., & Jenkins, J. E. (1983). Experimental Characterization of the Greenschist Amphibolite Boundary in Mafic Systems. *American Journal of Science*, 283(1), 48-92.
- Onions, R. K., & Gronvold, K. (1973). Petrogenetic Relationships of Acid and Basic Rocks in Iceland - Sr-Isotopes and Rare-Earth Elements in Late and Postglacial Volcanics. *Earth and Planetary Science Letters*, 19(4), 397-409.
- Palmer, M. R., & Edmond, J. M. (1989). The Strontium Isotope Budget of the Modern Ocean. *Earth and Planetary Science Letters*, 92(1), 11-26.
- Peate, D. W., Baker, J. A., Jakobsson, S. P., Waight, T. E., Kent, A. J. R., Grassineau, N. V., & Skovgaard, A. C. (2009). Historic magmatism on the Reykjanes Peninsula, Iceland: a snap-shot of melt generation at a ridge segment. *Contributions to Mineralogy and Petrology*, 157(3), 359-382. doi: Doi 10.1007/S00410-008-0339-4
- Raffone, N., Ottolini, L. P., Tonarini, S., Gianelli, G., D'Orazio, M., & Fridleifsson, G. O. (2010). *An investigation of trace and isotope light elements in minerals phases from well RN-17 (Reykjanes Peninsula, SW Iceland)*. Paper presented at the IOP Conf. Series: Materials Science and Engineering.
- Snæbjörnsdóttir, S. Ó. (2011). *Jarðfræði og jarðhitaummyndun við vesturjaðar sigdældar Hengils*. (Master), University of Iceland, Reykjavík. Retrieved from <http://hdl.handle.net/1946/10794>
- Steinthorsson, S., & Sveinbjörnsdóttir, A. E. (1981). Opaque Minerals in Geothermal Well No-7, Krafla, Northern Iceland. *Journal of Volcanology and Geothermal Research*, 10(1-3), 245-261.
- Sveinbjörnsdóttir, A. E. (1991). Composition of Geothermal Minerals from Saline and Dilute Fluids - Krafla and Reykjanes, Iceland. *Lithos*, 27(4), 301-315.
- Sæmundsson, K., 1995. Geological Map of Hengill
- Taylor, B. E., & Liou, J. G. (1978). Low-Temperature Stability of Andradite in C-O-H Fluids. *American Mineralogist*, 63(3-4), 378-393.
- Tomasson, J., & Kristman, H. (1972). High-Temperature Alteration Minerals and Thermal Brines, Reykjanes, Iceland. *Contributions to Mineralogy and Petrology*, 36(2), 123-&.

Tronnes, R. G. (1990). Basaltic Melt Evolution of the Hengill Volcanic System, Sw Iceland, and Evidence for Clinopyroxene Assimilation in Primitive Tholeiitic Magmas. *Journal of Geophysical Research-Solid Earth and Planets*, 95(B10), 15893-15910.

Appendix I

Table 7 Major and trace elements in HE-50 and HE- 51

Sample	HE-50 0	HE-50 -50	HE-50 -100	HE-50 -145	HE-50 -195	HE-50 -245	HE-50 -295	HE-50 -344	HE-50 -392	HE-50 -441	HE-50 -489	HE-50- 537	HE-50 -586	HE-50 -634	HE-50 -682	HE-50 -731	HE-50 -779
<i>Normalized major elements (wt.%)</i>																	
SiO ₂	49.67	48.56	49.69	47.66	48.74	50.18	48.50	50.04	49.76	53.85	51.20	52.96	52.53	50.08	49.89	52.07	50.63
Al ₂ O ₃	12.66	13.22	15.96	13.79	14.51	17.64	18.78	15.22	15.82	14.03	14.03	12.36	13.69	14.80	13.13	13.30	12.94
FeO*	14.36	14.42	13.76	14.86	12.40	9.51	8.92	10.15	11.19	8.62	9.45	11.94	9.87	10.03	11.04	10.83	11.29
MnO	0.23	0.25	0.21	0.30	0.24	0.17	0.18	0.18	0.24	0.16	0.17	0.23	0.17	0.18	0.21	0.20	0.20
MgO	6.27	5.98	7.56	6.31	5.92	4.36	4.56	5.70	5.14	4.86	5.79	6.05	5.80	6.66	7.32	6.13	6.91
CaO	10.24	11.28	8.76	11.50	11.51	13.72	14.11	13.48	12.98	13.97	14.19	11.00	12.96	13.86	13.45	12.07	12.78
Na ₂ O	2.48	2.56	0.75	1.59	2.67	1.82	2.26	2.16	2.02	1.47	2.35	1.75	2.20	2.19	1.98	2.21	2.27
K ₂ O	0.38	0.30	0.14	0.18	0.46	0.28	0.14	0.25	0.36	0.65	0.38	0.33	0.28	0.23	0.28	0.43	0.33
TiO ₂	2.65	2.44	2.28	2.67	2.47	1.63	1.77	1.98	1.73	1.64	1.74	2.40	1.78	1.39	1.95	1.93	1.88
P ₂ O ₅	0.49	0.45	0.35	0.62	0.54	0.32	0.36	0.40	0.32	0.35	0.33	0.51	0.27	0.18	0.28	0.35	0.30
<i>Normalized trace elements (ppm)</i>																	
Ba	105	110	63	73	151	74	62	86	88	218	108	111	60	53	68	110	84
Co	68	70	76	64	63	52	49	54	53	43	53	57	51	52	58	54	55
Cr	119	113	200	119	142	157	202	190	141	129	225	167	242	178	236	145	200
Cu	143	90	67	71	80	87	122	83	60	111	56	79	79	72	84	134	82
La	15	15	11	18	20	10	10	13	12	12	10	16	9	4	9	10	8
Ni	62	61	76	50	68	70	68	68	51	44	60	59	61	70	75	58	60
Sc	44	44	50	43	42	34	41	39	40	33	36	42	43	45	50	43	49
Sr	317	237	143	207	243	280	256	364	239	246	224	212	183	204	212	220	217
Y	44	40	39	49	41	27	31	31	35	30	28	45	30	23	31	35	32
Zn	113	129	153	120	104	82	76	87	85	75	75	105	87	74	81	84	79
Zr	171	152	137	184	163	144	119	126	107	101	100	293	100	83	108	120	104

Table 7 Major and trace elements in HE-50 and HE- 51

Samples	HE-50 -779	HE-50 -827	HE-50 -876	HE-50 -924	HE-50 -972	HE-50 -1021	HE-50 -1070	HE-50 -1118	HE-50 -1167	HE-50 -1216	HE-50 -1265	HE-50 -1313	HE-50 -1363	HE-50 -1450	HE-50 -1460	HE-50 -1509	HE-50 -1559	HE-50 -1607
<i>Normalized major elements (wt.%)</i>																		
SiO ₂	50.63	49.46	50.01	51.83	50.20	50.45	49.77	51.07	50.42	49.50	49.93	50.21	49.33	49.46	49.67	49.73	49.04	48.62
Al ₂ O ₃	12.94	14.73	12.06	12.60	12.94	13.03	12.13	12.95	13.56	12.89	13.52	12.26	13.78	14.57	14.60	12.91	13.59	13.75
FeO*	11.29	10.98	12.34	11.87	12.87	12.35	12.31	11.69	11.21	13.09	11.15	12.98	11.16	11.09	11.10	12.53	12.03	11.52
MnO	0.20	0.20	0.22	0.21	0.23	0.22	0.23	0.21	0.20	0.23	0.20	0.24	0.21	0.20	0.20	0.23	0.21	0.22
MgO	6.91	6.45	6.80	6.39	6.25	6.34	7.13	6.64	6.91	6.51	7.63	6.46	7.58	7.00	7.38	6.92	7.31	7.88
CaO	12.78	12.79	12.40	11.07	11.53	11.33	12.35	12.01	12.41	11.62	12.12	11.71	13.31	12.71	12.08	11.79	12.09	13.10
Na ₂ O	2.27	2.38	2.37	2.29	2.24	2.52	2.58	2.25	2.28	2.50	2.72	2.47	2.02	2.40	2.33	2.59	2.54	2.15
K ₂ O	0.33	0.29	0.37	0.46	0.39	0.40	0.33	0.42	0.31	0.34	0.23	0.35	0.17	0.27	0.18	0.21	0.18	0.20
TiO ₂	1.88	1.97	2.48	2.30	2.40	2.38	2.27	1.96	1.92	2.34	1.77	2.40	1.75	1.61	1.73	2.20	2.19	1.91
P ₂ O ₅	0.30	0.29	0.40	0.48	0.44	0.47	0.35	0.30	0.30	0.44	0.24	0.40	0.22	0.26	0.29	0.37	0.34	0.18
<i>Normalized trace elements (ppm)</i>																		
Ba	84	75	95	112	105	100	93	85	90	96	55	92	47	77	64	78	70	47
Co	55	54	59	58	63	61	60	56	57	62	55	63	55	53	55	60	59	58
Cr	200	170	177	152	123	109	137	144	210	108	203	115	204	152	176	121	164	213
Cu	82	123	123	109	100	96	108	128	104	128	125	115	116	132	125	136	158	111
La	8	9	12	14	15	14	12	10	11	35	9	15	8	11	8	11	9	5
Ni	60	65	58	58	54	49	58	66	71	56	76	54	76	58	82	60	70	98
Sc	49	47	53	48	47	47	53	48	46	48	51	49	52	46	45	49	47	50
Sr	217	215	221	227	228	230	223	219	215	212	209	203	194	220	212	213	235	202
Y	32	32	40	44	40	41	38	34	33	42	34	44	28	26	32	39	33	24
Zn	79	82	89	86	93	96	88	86	80	99	82	98	86	83	82	94	94	89
Zr	104	107	143	153	149	159	130	110	113	145	99	153	87	93	105	128	119	76

Table 7 Major and trace elements in HE-50 and HE- 51

Samples	HE-50 -1607	HE-51 121	HE-51 85	HE-51 51 35	HE-51 -15	HE-51 -75	HE-51 -122	HE-51 -161	HE-51 -208	HE-51 -251	HE-51 -295	HE-51 -338	HE-51 -382	HE-51 -425	HE-51 -468	HE-51 -510	HE-51 -552	HE-51 -595
<i>Normalized major elements (wt.%)</i>																		
SiO ₂	48.62	57.68	54.21	51.81	54.64	49.41	52.36	50.71	49.80	50.83	52.98	49.96	53.48	50.78	51.65	50.93	50.18	49.22
Al ₂ O ₃	13.75	10.60	13.34	12.59	13.88	13.67	14.98	13.65	15.00	16.36	12.36	12.33	14.69	13.26	12.16	13.73	12.62	14.76
FeO*	11.52	11.83	11.39	17.31	9.92	10.69	11.80	10.60	12.13	9.51	11.82	14.44	9.62	11.22	10.75	10.41	12.34	10.96
MnO	0.22	0.12	0.23	0.32	0.16	0.18	0.24	0.19	0.22	0.17	0.21	0.24	0.20	0.22	0.21	0.20	0.23	0.19
MgO	7.88	3.71	3.64	3.34	5.54	5.81	4.97	6.02	6.04	4.73	5.22	4.52	4.38	4.66	6.27	6.18	6.72	6.79
CaO	13.10	10.59	10.07	7.26	11.33	14.87	9.23	13.69	11.47	13.29	11.43	10.51	11.10	14.15	14.16	12.34	12.22	12.78
Na ₂ O	2.15	1.24	2.31	2.21	1.93	2.09	2.75	2.17	2.15	2.38	2.16	3.44	2.92	1.90	1.48	2.55	2.10	2.37
K ₂ O	0.20	0.91	0.82	0.75	0.15	0.17	0.42	0.10	0.14	0.18	0.48	1.11	0.88	0.62	0.82	0.53	0.34	0.28
TiO ₂	1.91	2.23	2.79	2.83	1.76	2.15	2.19	1.98	2.16	1.79	2.36	2.14	1.77	2.25	1.68	2.27	2.29	1.90
P ₂ O ₅	0.18	0.69	0.79	1.26	0.32	0.53	0.64	0.48	0.39	0.36	0.55	0.98	0.62	0.49	0.39	0.40	0.44	0.29
<i>Normalized trace elements (ppm)</i>																		
Ba	47	164	182	211	52	58	164	45	48	68	131	264	173	120	164	122	113	68
Co	58	58	59	56	53	55	51	54	59	52	57	46	40	53	49	53	62	56
Cr	213	104	43	14	106	116	118	188	126	242	91	97	125	175	246	129	239	208
Cu	111	87	54	55	113	74	71	71	127	103	69	30	41	68	160	56	114	95
La	5	22	26	36	10	18	27	18	13	17	19	37	25	17	14	13	14	9
Ni	98	47	18	15	58	56	39	57	59	64	33	18	34	45	72	45	78	61
Sc	50	33	31	26	37	35	36	39	45	42	36	31	29	36	33	45	45	45
Sr	202	209	285	355	230	340	258	212	225	230	267	395	282	229	233	276	238	230
Y	24	47	51	67	24	36	55	38	37	33	43	72	48	41	31	35	39	31
Zn	89	101	102	129	87	89	111	89	98	80	103	121	93	95	84	91	105	81
Zr	76	158	219	336	108	150	252	161	135	106	184	318	216	171	121	139	148	115

Table 7 Major and trace elements in HE-50 and HE- 51

Samples	HE-51-595	HE-51-638	HE-51-681	HE-51-724	HE-51-767	HE-51-810	HE-51-853	HE-51-896	HE-51-939	HE-51-982	HE-51-1025	HE-51-1068	HE-51-1111	HE-51-1154	HE-51-1197	HE-51-1240	HE-51-1283	HE-51-1326
<i>Normalized major elements (wt.%)</i>																		
SiO ₂	49.22	50.78	49.97	50.46	52.72	49.86	49.51	52.07	50.75	50.16	50.78	50.18	51.21	50.64	49.81	50.56	49.81	52.02
Al ₂ O ₃	14.76	13.55	13.48	13.58	12.69	12.57	14.84	12.74	13.14	11.90	11.68	11.78	12.69	12.85	13.43	12.27	14.25	11.75
FeO*	10.96	10.85	10.62	11.45	11.06	12.65	10.28	12.46	11.73	12.39	11.63	12.24	11.79	12.22	11.76	11.89	10.16	11.98
MnO	0.19	0.19	0.20	0.21	0.19	0.23	0.18	0.23	0.22	0.22	0.21	0.23	0.22	0.22	0.20	0.23	0.19	0.22
MgO	6.79	6.76	7.29	6.46	5.63	6.63	6.86	5.81	6.13	7.26	7.44	6.85	6.09	6.55	6.68	6.59	7.31	6.46
CaO	12.78	12.68	14.32	11.90	12.90	12.48	14.07	10.63	12.05	12.41	13.00	12.71	11.88	12.03	12.04	11.78	12.79	11.40
Na ₂ O	2.37	2.28	1.51	2.52	1.71	2.09	1.84	2.04	2.52	2.32	2.29	2.48	2.70	2.34	2.73	2.74	2.70	2.68
K ₂ O	0.28	0.30	0.33	0.33	0.28	0.29	0.22	0.37	0.33	0.34	0.32	0.35	0.44	0.30	0.31	0.45	0.31	0.46
TiO ₂	1.90	1.86	1.65	2.18	2.00	2.31	1.53	2.60	2.20	2.13	1.89	2.29	2.12	2.03	2.20	2.55	1.78	2.14
P ₂ O ₅	0.29	0.31	0.22	0.45	0.35	0.38	0.23	0.57	0.46	0.37	0.27	0.35	0.36	0.35	0.35	0.45	0.25	0.38
<i>Normalized trace elements (ppm)</i>																		
Ba	68	85	66	103	93	84	55	134	91	93	84	90	112	77	82	113	79	117
Co	56	53	52	56	58	64	51	60	57	62	59	61	57	60	60	58	52	58
Cr	208	240	230	141	106	108	265	90	131	194	160	168	92	118	150	160	223	117
Cu	95	74	118	78	62	70	64	57	63	64	134	130	120	146	135	98	127	136
La	9	9	6	15	12	14	8	16	17	11	8	14	12	10	10	15	6	11
Ni	61	64	77	59	47	47	66	45	46	65	62	58	46	56	58	51	71	57
Sc	45	46	48	44	42	48	47	42	43	51	53	53	48	49	49	49	48	47
Sr	230	218	191	229	215	227	200	241	239	224	219	219	219	210	238	244	238	215
Y	31	34	28	39	34	38	27	52	41	37	32	42	42	38	37	43	28	39
Zn	81	81	71	93	91	101	72	102	94	90	91	95	93	93	91	100	77	91
Zr	115	117	90	156	125	139	86	184	206	130	116	146	150	125	129	174	94	134

Table 7 Major and trace elements in HE-50 and HE- 51

Samples	HE-51 -1326	HE-51 -1369	HE-51 -1412	HE-51 -1455	HE-51 -1498	HE-51 -1541	HE-51 -1584	HE-51 -1627	HE-51 -1670	HE-51 -1713	HE-51 -1756	HE-51 -1799	HE-51 -1842	HE-51 -1885	HE-51 -1928
<i>Normalized major elements (wt.%)</i>															
SiO ₂	52.02	49.78	53.08	49.97	49.51	49.34	49.91	49.51	51.03	49.85	49.27	49.34	48.90	49.69	49.54
Al ₂ O ₃	11.75	12.56	13.54	12.00	13.43	12.16	13.56	13.07	12.82	12.51	13.60	13.36	13.02	11.30	12.88
FeO*	11.98	11.81	10.70	12.61	12.02	12.58	11.71	11.85	11.90	12.02	12.00	12.45	13.51	13.55	12.59
MnO	0.22	0.21	0.22	0.24	0.22	0.23	0.22	0.22	0.23	0.22	0.22	0.23	0.23	0.25	0.23
MgO	6.46	7.39	5.99	6.99	7.10	7.28	6.84	7.36	6.59	7.35	7.13	7.17	6.71	6.67	6.83
CaO	11.40	12.64	9.95	12.06	12.48	12.38	12.33	12.70	11.02	12.83	12.70	12.09	12.50	12.25	12.06
Na ₂ O	2.68	2.45	3.28	2.64	2.31	2.51	2.45	2.36	3.27	2.21	2.21	2.25	2.12	2.41	2.66
K ₂ O	0.46	0.34	0.68	0.35	0.27	0.38	0.25	0.29	0.34	0.24	0.26	0.33	0.32	0.34	0.30
TiO ₂	2.14	2.01	1.72	2.25	1.87	2.25	1.94	1.87	1.96	1.98	1.85	1.99	1.90	2.57	2.09
P ₂ O ₅	0.38	0.30	0.48	0.36	0.30	0.36	0.32	0.29	0.36	0.29	0.28	0.31	0.33	0.42	0.32
<i>Normalized trace elements (ppm)</i>															
Ba	117	79	160	89	79	97	71	68	95	67	66	70	83	93	78
Co	58	58	46	61	58	60	56	58	57	61	58	61	57	63	61
Cr	117	137	173	95	130	186	136	156	122	158	165	169	267	138	135
Cu	136	155	86	156	159	141	125	118	134	134	130	125	111	133	137
La	11	8	22	11	10	11	12	10	15	10	10	11	13	15	12
Ni	57	61	63	52	63	62	59	66	67	67	71	73	76	58	66
Sc	47	52	39	52	49	52	48	51	47	52	50	48	46	53	49
Sr	215	216	247	214	212	215	200	194	217	189	194	203	198	209	212
Y	39	33	54	40	34	38	38	33	44	34	32	37	35	44	38
Zn	91	84	99	94	89	93	93	85	90	86	87	88	102	104	92
Zr	134	109	234	133	111	130	132	104	151	107	107	197	125	153	124

Appendix II

Table 8 Represent prehnite analyses from Hellisheiði Geothermal Field

Well	HE-50	HE-50	HE-50	HE-51	HE-51	HE-50	HE-50
Depth	-1412	-1021	-1021	-295	-295	-1559	-1559
SiO ₂	42.96	43.11	43.57	43.13	42.47	42.27	42.49
Al ₂ O ₃	22.64	20.37	23.40	22.68	20.91	19.70	20.29
Fe ₂ O ₃	1.94	5.94	2.39	1.11	4.25	3.93	6.71
CaO	27.30	26.88	27.42	26.91	26.77	27.07	26.37
Total	95.26	96.59	96.88	94.37	94.90	93.59	96.24
Si	3.000	3.000	2.980	3.030	3.000	3.053	3.014
Al	1.860	1.670	1.890	1.880	1.740	1.677	1.697
Fe ³⁺	0.100	0.310	0.120	0.060	0.230	0.238	0.398
Ca	2.040	2.010	2.010	2.020	2.030	2.095	2.004
Total	7.000	6.990	7.000	6.990	7.000	7.063	7.113